Indian Journal of Pure & Applied Physics
Vol. 52, May 2014, pp. 293-313

Review Article

Review on Se-and S-doped hydrogenated amorphous silicon thin films

Sanjeev K Sharma[1]*, Hyunsik Im[1], Deuk Young Kim[1] & R M Mehra[2]
[1]Department of Semiconductor Science, Dongguk University-Seoul, Jung-gu, Seoul 100-715, Republic of Korea
[2]School of Engineering and Technology, Sharda University, Knowledge Park-III, Greater Noida, India
*E-mail: sksharma@dongguk.edu, dykim@donggyu.edu

Received 17 July 2013; revised 26 December 2013; accepted 5 March 2014

Hydrogenated amorphous silicon thin films manufactured by plasma deposition techniques are widely used in electronic and optoelectronic devices. The optical and electrical properties of undoped and doped hydrogenated amorphous silicon (a-Si:H) thin films determine the importance and characteristics of the final film structure of practical devices. In particular, a-Si:H thin film solar cells and optical sensors have many industrial and technical advantages, such as being light weight, low cost, and having a large deposition area. The a-Si:H thin film is one of the candidates for flexible solar cells for use in space. This article reviews the optical and electrical properties of double donor Se-and S-doped a-Si:H thin films, which can be considered as an alternative to wide bandgap absorbing layers in the next generation of optoelectronic devices.

Keywords: Hydrogenated amorphous silicon, Double donor, Optical properties, Electrical properties, Conduction mechanism

1 Introduction

1.1 Silicon (Si)

Silicon is the 8th most common element in the universe by mass, but very rarely occurs in nature as the pure free element. It is more widely distributed in dusts, sands, planetoids and planets, as various forms of silicon dioxide (silica) or silicates. In the Earth's crust, silicon is the second most abundant element after oxygen (46.6%), making up 27.7% of the crust by mass[1,2]. Silicon is the principal component of most semiconductor devices, most importantly integrated circuits or microchips[3]. Also, its native oxide is easily grown in a furnace, and forms a good semiconductor/ dielectric interface[4]. Pure silicon is not a conductor, because there are no free electrons; all the electrons are tightly bound to neighbouring atoms. To make silicon conducting, producers combine or ‘dope’ pure silicon with very small amounts (1 millionth atom) of other elements, like boron (B for *p*-type), or phosphorus (P for *n*-type). Phosphorus has five outer valence electrons. When three silicon atoms and one phosphorus atom bind together in the basic silicon crystal cell of four atoms, there is an extra electron and a net negative charge[5-8]. Boron is then incorporated into a threefold coordinated site, and bonds to the neighbouring Si atoms much like any Si atom, except that it has one less nuclear charge and one less electron. Thus, a shallow acceptor state is created near the valence-band edge and there is one fewer electron to fill the electronic states. Thus, at least at low or moderate temperatures as more B is incorporated, the Fermi level moves down towards the valence-band edge[9,10].

1.2 Crystalline silicon (c-Si)

Crystalline silicon (c-Si) is the foundation of today’s rapidly growing photovoltaic (PV) industry[11], and is available in the form of crystalline wafers for practical devices. Silicon appears to be the near-ideal PV material, as it is abundant, non-toxic, and benefits from an enormous knowledge base and industrial infrastructure. The c-Si films can be readily grown by depositing amorphous silicon (a-Si:H) on glass, and subsequently annealing the films[12] at 550-600°C for 6-24 h. The greatest challenge is likely to be the high interfacial reactivity of the Si and SiO_2. Nonetheless, silicon epitaxy has been achieved on a number of foreign substrates[13]. Photovoltaic solar cells will likely require epitaxial thickening to 2-10 μm and effective light trapping to reach efficiencies of 15% or higher[14].

1.3 Amorphous silicon (a-Si)

The term ‘amorphous’ is commonly applied to non-crystalline (non-ordered) materials prepared by deposition from gases. The chemical bonding of atoms in non-crystalline materials is nearly unchanged from that in crystals[15]. Amorphous materials are disorderly varied in the angles between the bonds and the regular lattice structure is eliminated. Interest in amorphous semiconductors

developed around the chalcogenides, which are materials containing the elements sulphur (S), selenium (Se) and tellurium (Te); examples are As_2Se_3, and GeS_2. In the seventies, it was discovered that amorphous silicon (a-Si) is suitable as a semiconductor in solar cells, although lower yields are achieved with it. Amorphous silicon was different from crystalline (ordered) silicon (c-Si), in terms of device characteristics. At the point when no crystals need to be formed, a material that could be processed at far lower temperatures (~200°C) onto a variety of substrates offered some unique capabilities for a variety of electronics[16-20]. The loss of structure results in defects, such as dangling bonds and distorted Si-Si bonds (in both lengths and angles). Defects yield energy levels in the energy gap where electrons recombine with holes, thus limiting the flow of current[21-26], which could be suppressed by the incorporation of hydrogen.

1.4 Hydrogenated amorphous silicon (a-Si:H)

Silicon (Si) and hydrogen (H) are extremely abundant in nature. Hydrogen incorporation in silicon layers prepared by PECVD using silane (SiH_4) dilution reduced the defects in amorphous silicon[27-29]. The hydrogen caused a similar improvement in the material properties, as was found for glow discharge a-Si:H, with a high photoconductivity, low defect density and calm doping[30-32]. Research on both glow discharge and sputtered a-Si:H has continued[33-35], but the glow discharge technique has become increasingly dominant, because it seems to give slightly better material properties[36-40]. The material is easily (although not efficiently) doped with both *p*- and *n*-type using boron[9,41] and phosphorus[41-43] sources, respectively. The material possesses low dark conductivity and excellent photoconductivity. The material allows bandgap profiling by alloying with different elements; bandgap can be decreased to 1.0 eV by alloying[44-46] with Ge (a-Si,Ge:H); and can be increased to as high as 3.6 eV, by alloying[46-50] with C (a-Si,C:H). The material allows easy deposition of heterojunction structure[51-59].

Hydrogenated amorphous silicon is a promising material since it was introduced in the seventies, and its usefulness has continued to date, for hybrid solar cells[39,45,53,60-64], switching devices[65], digital X-ray and optical imaging[66], visible photoluminescence[47,67-70], thin film transistors[71-73], photosensors for the detection of bio-molecules[74,75], micro-electro-mechanical systems[76,77] (MEMSs), gas sensors[78,79], pixel detectors for high energy particles[80,81], photodetectors[59], and so forth. Hydrogenated amorphous silicon thin films and its alloys are promising contenders for the realization of advanced opto-electronic devices. Fig. 1 shows schematic illustrations of crystalline silicon [Fig. 1(a)] and hydrogenated amorphous silicon [Fig. 1(b)]. In the case of ideal a-Si:H, all the hydrogen is singly coordinated and the silicon is four-fold coordinated. Many properties of amorphous materials can be defect controlled, such as magnetic properties, optoelectronic behaviour, vibrational properties and mechanical characteristics. For some materials such as chalcogenide glasses, it is impossible to experimentally achieve the ideal amorphous state, as structural defects are present even in thermal equilibrium in the melt, and are consequently frozen-in on solidification.

1.5 Advantages of a-Si:H over c-Si

Hydrogenated amorphous silicon (a-Si:H) based technology for optoelectronic devices is relatively simple and inexpensive, compared with crystalline silicon (c-Si) based technology[82]. For a given layer thickness, a-Si:H absorbs much more energy[83] than c-Si (about 2.5 times the amount). Much less material is required to prepare a-Si:H films, which are lighter in weight, and less expensive. Hydrogenated amorphous silicon can be deposited on a wide range of substrates, including flexible, curved, and roll-away types. The disordered atomic structure and the presence of hydrogen combine to give new phenomena, which are strikingly different from those in the crystalline semiconductors. The structural disorder results in localized band tail states that are characteristic of amorphous materials, which are reflected in the optical, transport and recombination properties; while the hydrogen gives unique defect, doping and metastability effects[84-86]. Recently, experimental modules have been introduced of hydrogenated

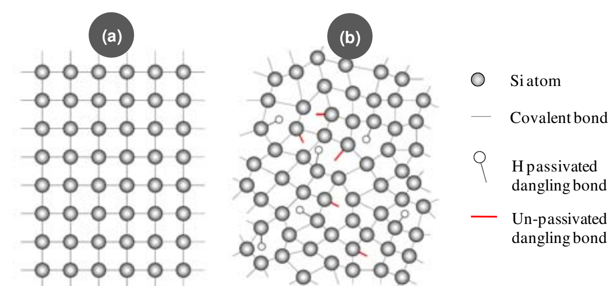

Fig. 1 — Schematic illustration of the atomic structure of (a) single crystal silicon (c-Si) (b) hydrogenated amorphous silicon (a-Si:H)

nano/micro-crystalline silicon (*n*/μc-Si:H) solar cell[38,87-90], which are based on a combination of a-Si:H solar cells. Table 1 presents the basic properties (bandgap, density, work function, electron/hole mobility) of crystalline silicon and hydrogenated amorphous silicon.

1.6 Advantages of double donor Se-and S-doped a-Si:H

It has been recognized that the lengthy lighting of a-Si:H with bandgap light reduces photoconductivity[91]. It has been suggested that light-induced reduction in photoconductivity may be caused by the creation of metastable recombination centers in the gap. This behaviour can be a limiting factor in optoelectronic applications of a-Si:H. Based on the data for crystalline silicon (c-Si) doped with chalcogens[92,93] and the passivation of these dopants by hydrogen, the qualitativety[94,95] of a-Si:H can be understood. With the application of band-gap light, it has been assumed that these donors can be activated optically. This involves the optical alteration of S sites that have been passivated by hydrogen. Again, judging from the c-Si, the optical activation should be more efficient for sulphur than for P (group V element). As a result of this activation, the illumination increases the dark and photo conductivities, and the Fermi level moves towards the conduction band edge. This metastable increase is similar to that which is termed as persistent photoconductivity, which occurs in some compensated films of Se and S doped[96] a-Si:H, modulated films[97], and multilayer heterostructures[98-100] of a-Si:H. The energy levels are even shallower (80-135 meV) for S-related complexes[101] in Si. These data clearly indicate that there are several possibilities for the incorporation of sulphur as a donor in a-Si, S_x:H alloys. Indeed, the hydrogen passivation of S_2 (double donors) is much more effective than the group V donors[102] (for example, P and As). The doping of double donors of group VI elements such as Se or S in a-Si:H showed significant reduction in the degradation of photoconductivity[103-105]. Sharma *et al.*[106,107] have investigated the effect of Se or S doping on a-Si:H and studied the change in conduction mechanism with temperature. The use of Se and S as dopants in a-Si:H thin films grown by capacitively coupled *RF* glow discharge decomposition of silane (SiH_4), hydrogen sulphide (H_2S) and hydrogen selenide (H_2Se) diluted in helium (He) results in silicon dangling bonds being terminated in the same way as hydrogen[108]. Hydrogenated amorphous silicon is the basis of an expanding large-area-electronics industry, which started with solar cells for consumer electronic devices, and today covers an expanding number of applications. The effect of composition and annealing on the optical properties of Se or S-doped a-Si:H should be considered when evaluating their operational characteristics[109].

Table 1 — Properties of a-Si:H and c-Si

Material	Density (g/cm^3)	Band gap (eV)	W (eV)	Electron mobility (cm^2/Vs)	Hole mobility (cm^2/Vs)
c-Si	2.30	1.1	3.6	1350	480
a-Si:H	2.25	1.7	4 ~ 4.8	2 ~ 5	0.005

2 Experimental Details

2.1 Growth of the films

A variety of deposition techniques can be used for the deposition of hydrogenated amorphous silicon thin films. Most of these techniques are slight variations of the main processing technologies, namely chemical vapour deposition (CVD), pulsed laser deposition (PLD), laser ablation deposition (LAD) and sputtering techniques. Among these techniques, CVD is the most frequently utilized family of techniques, which at high deposition temperatures produces the crystalline phase and at low deposition temperatures yields the amorphous phase. Plasma-enhanced chemical vapour deposition (PECVD) is the most commonly used process from the CVD family for the deposition of a-Si:H. There are other studies that report on the deposition of thin film a-Si:H using Hot Wire Chemical Vapour Deposition[110] (HWCVD) and Electron Cyclotron Resonance (ECR) CVD. The HWCVD approach, besides permitting low substrate temperatures, features resistive heating of the 'hot' wire and accordingly catalytic decomposition of the precursor gases on the wire as a parameter to control the ion-free deposition of a-SiC:H with implications in the tuning of its bandgap[111].

2.1.1 Plasma-enhanced chemical vapour deposition (PE-CVD)

This process was used to deposit hydrogenated amorphous silicon thin films from a gas state (vapour) to a solid state on a substrate at a specified substrate temperature. The chemical reactions were involved in the process, which occur after creation of plasma of the reacting gases. The plasma is,generally, created by *RF* (*ac*) frequency or *dc* (direct current) discharge

between two electrodes, the space between is filled with the reacting gases. Hydrogenated amorphous silicon-sulphur and silicon-selenium alloy (a-Si,S:H and a-Si,Se:H) thin films were prepared by glow discharge (13.56 MHz) plasma-enhanced chemical vapour deposition (PE-CVD) decomposition of hydrogen selenide (H_2Se) and hydrogen sulphide (H_2S) vapours mixed with silane (SiH_4) to produce *n*-type amorphous silicon[105-109,112,113,]. Depositions were performed on Corning 7059 highly clean glass substrate at a temperature of 230°C. The base pressure of the chamber was manipulated to be low 10^{-7} mbar range. The silane flow rate was kept constant at 10 sccm, while the gas phase doping concentration was controlled by varying the H_2Se or H_2S/H_2 flow rate. The pressure of the gas mixture during deposition was about 0.1 to 0.3 torr and low *RF* power was employed to obtain deposition rates of 1-2Å/s.

2.1.2 Pulsed laser deposition (PLD)

Conceptually and experimentally, pulsed laser deposition (PLD) is an extremely simple technique, probably the simplest among all thin film growth techniques. It consists of a target holder and a substrate holder housed in a vacuum chamber. A high-power laser is used as an external energy source to vapourize materials and deposit thin films. A set of optical components is used to focus and raster the laser beam over the target surface. The decoupling of the vacuum hardware and the evaporation power source makes this technique so flexible that it is easily adaptable to different operational modes without the constraints imposed by the use of internally powered evaporation sources. The advantages of pulsed laser ablation are flexibility, fast response, energetic evaporants and congruent evaporation. The process of PLD can,generally, be divided into four stages: (i) laser ablation of the target material and creation of a plasma, (ii) dynamic of the plasma, (iii) deposition of the ablation material on the substrate, (iv) nucleation and growth of the film on the substrate surface. However, this technique can be usually used for ceramic materials thin films (YBCO, PZT, SBN etc.), hard coatings[114-118] (diamond/diamond like films e.g. TiC, SiC, CN, SiO2, TiN, BN, etc.). Lengsfeld *et al*[119]. used to deposit a-Si:H with a hydrogen content of 10 at.% which were crystallized employing a step-by-step crystallization method.

2.2 Characterization of the films

The selenium-silicon and sulphur-silicon concentrations (Se/Si and S/Si) were determined by electron microprobe measurements. The thicknesses of the films as measured by surface profiler (DekTaK3), were in the range 2.21-5.44 μm for selenium and 0.24-2.27 μm for sulphur samples. Bonding structure in the alloy was investigated using IR absorption spectra. The IR spectra revealed that the main effect of S and Se alloying is a strong increase in the strength of the mode at approximately 480 cm^{-1}, which corresponds to Si-S bond[120] and at about 390 cm^{-1}, corresponding to Si-Se bond[121]. Table 2 presents the detail of the samples for example the doping gas ratio (H_2Se/SiH_4 and H_2S/SiH_4) and the selenium/silicon (Se/Si) and sulfur/silicon (S/Si) concentrations.

2.2.1 X-ray diffraction

Amorphous materials are often defined operationally by their diffraction patterns. That is, the diffraction patterns consist of a few broad halos rather than sharp Bragg reflections. However, markedly different structures can also lead to qualitatively the same diffraction patterns. A small crystallite size, strains, imperfections, broaden the normally sharp crystallite reflections and as the crystal size gets smaller a point is reached where the crystalline reflections overlap and the diffraction pattern appears like that for an amorphous materials. The crystalline size at which the diffraction pattern appears amorphous has been discussed by Germer and White[122] and Piggott[123] and is approximately four unit cells in diameter for monatomic close packed materials. Thus, diffraction cannot distinguish between a random arrangement of atoms, as suggested by Bernal[124] for monatomic systems and Zacharison[125] for polyatomic systems, and a microcrystalline one, where each micro crystalline contains approximately two hundred atoms. Indeed, because of this, microcrystalline

Table 2 — Details of the samples prepared: the selenium and sulphur concentrations (Se/Si and S/Si), doping gas ratio (H_2Se/SiH_4 and H_2S/SiH_4) [Ref.109]

	Sample	H_2Se/SiH_4 (Doping gas ratio)	Se/Si gas (Doping Concentrations)
a-Si,Se:H	Se-1	1.0×10^{-1}	2.50×10^{-1}
	Se-2	1.0×10^{-2}	2.01×10^{-2}
	Se-3	1.0×10^{-3}	2.18×10^{-3}
	Se-4	1.0×10^{-4}	1.60×10^{-4}
		(H_2S/SiH_4)	S/Si
a-Se,S:H	S-2	2.0×10^{-2}	
	S-4	1.0×10^{-4}	1.20×10^{-3}
	S-5	1.1×10^{-5}	1.80×10^{-4}
	S-6	6.8×10^{-7}	1.70×10^{-6}

models for the amorphous state had been proposed for polyatomic system by Valenkov and Porai-Koshits[126] and for monatomic system by Mott and Khalid[127,128]. The absence of sharp peaks in X-ray diffraction (XRD Phillips-Holland Diffractometer, model X pert PRO) patterns of Se and S-doped a-Si:H films confirmed the amorphous nature of the films.

2.2.2 Ultraviolet-visible (UV-VIS) spectroscopy

UV-Vis spectroscopy refers to absorption/ reflectance spectroscopy in the ultraviolet-visible spectral region (200-700 nm). This means it uses light in the visible and adjacent (near-UV and near-infrared (NIR)) ranges. UV-VIS spectroscopy is routinely used in the quantitative determination of solutions of transition metal ions highly conjugated organic compounds and biological macromolecules.

For the determination of optical properties, the transmission spectra of Se- and S-doped a-Si:H films were taken, using a UV-Vis double beam spectrophotometer (Shimadzu 260) having a resolution of ±1 nm in the wavelength[107,109] range 190-1100 nm. Fig. 2(a and b) shows the typical transmission spectra with a typical gas ratio of H_2Se/SiH_4 and $H_2S/SiH_4=1\times10^{-4}$, respectively. The transmission spectra were recorded in the as grown and annealed thin films[109].

UV-Vis spectrometer can also be used for the determination of thin film thickness of transparent films with Fourier-algorithms by using the phenomenon of white-light interference. The interference occurs at the optical boundaries of the transparent layers when a portion of light is reflected, and two or more light rays from the broadband light source interact with each other. Interference occurs if the layers are transparent, smooth, and parallel, allowing both reflected signals to interact. The resulting interference pattern varies according to the phase difference of the light waves, where different layer thicknesses induce varying phase differences of the back-scattered light[129].

2.2.3 FT-Raman spectroscopy

Raman spectroscopy is a method of determining modes of molecular motions, especially vibrational and rotational energy level structure. It is predominantly applicable to the qualitative and quantitative analyses of covalently bonded molecules[130]. As opposed to fluorescence methods, which require the addition of a separate fluorescing molecule as a 'tag' attached to the actual molecule of interest, Raman spectroscopy allows direct detection of a molecule with no chemical alteration[131-133].

2.2.4 X-ray photoemission spectroscopy (XPS)

XPS is the most widely used surface analysis technique because of its relative simplicity in use and data interpretation. The sample is irradiated with mono-energetic X-rays causing photoelectrons to be emitted from the sample surface. An electron energy analyzer determines the binding energy of the photoelectrons. From the binding energy and intensity of a photoelectron peak, the elemental identity, chemical state and quantity of an element are determined. XPS spectra are obtained by irradiating a material with a beam of X-rays while simultaneously measuring the kinetic energy and number of electrons that escape from the top 0 to 10 nm of the material being analyzed. XPS requires high vacuum (10^{-8} millibar) or ultra-high vacuum (UHV; pressure < 10^{-9} millibar) conditions, although a current area of development is ambient-pressure XPS, in which samples are analyzed at pressures of a few tens of millibar[134].

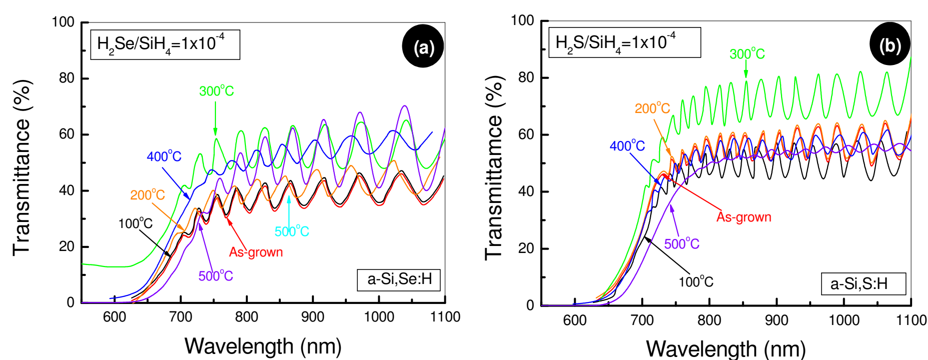

Fig. 2 — Typical transmission spectra of Se- and S-doped hydrogenated amorphous silicon (a-Si,Se:H and a-Si,S:H) thin films in the wavelength range from 600 to 1100 nm for as grown and the annealing temperatures in the range from 100° to 500°C (a) $H_2Se/SiH_4=1\times10^{-4}$ and (b) $H_2S/SiH_4=1\times10^{-4}$. Reproduced with permission from the authors of ref. 109; Copyright 2010, Elsevier

XPS is a useful tool for analyzing the elemental composition of undoped and doped hydrogenated amorphous silicon. X-ray irradiation-and annealing-induced structural changes in undoped hydrogenated amorphous silicon (a-Si:H) and pure amorphous silicon (a-Si) have been investigated in detail by X-ray photoemission spectroscopy (XPS). The irradiation-induced shifts of both the Si2s and Si2p peaks of a-Si:H are found to be unstable even at room temperature. They can be reversed by annealing, following a stretched exponential time dependence with a lower activation energy than that for the meta stable changes in electronic properties[135] (Staebler-Wronski effect). Toneva *et al*[136]. recorded the XPS-spectra of a-Si:H films of as-grown and light soaking by white light illumination (100 mW/cm^2) and observed Si2p, O1s and C1s elements. The change of the position and intensity of the Si2p peak was observed after light soaking and explained by the transformation of the Si-H bonds.

Yelon *et al*[137]. measured XPS-spectra of a-Si:H film after white light illumination and detected the shifting of both peaks Si2p and Si2s to lower binding energies by equal amounts. They calculated the preliminary density function on a simple model of a-Si:H and occurred the metastable expansion, such as elongations of the length of compressed Si-Si bonds and variations in the Si-Si-Si dihedral angle. The metastable expansion associated to be shift of XPS peak unidirectional. The chemical composition of *n*-doped a-Si:H films was evaluated by XPS up to five SiN layers (R = NH_3/SiH_4 = 2, 3.5, 4.5, 7.7, 10) deposited on *p*-type CZ c-Si substrates[138,139] (ρ = 100 Ωcm- NA=1.4×10^{15} cm^{-3}). Anandan *et al*[140]. investigated the interfacial reactions between aluminium and native-oxide-covered hydrogenated amorphous silicon. Core-level spectra of silicon and aluminium indicated the reduction of the native silicon oxide by the deposition of aluminium. The presence of a graded interface of suboxides of silicon acted as a diffusion barrier for further reaction. Sheng *et al*[141]. performed the depth profiling measurements across the back *n*-layer/transparent conducting oxide (*n*/TCO) interfaces for substrate *p*-i-*n* solar cells to examine differences between amorphous silicon (a-Si:H) and microcrystalline silicon (μc-Si:H) *n*-layer materials as well as TCO materials ZnO and ITO in the chemical, microstructural and diffusion properties of the back interfaces. They observed *n*-a-Si:H interfaces better with ITO, while *n*-μc-Si:H, with ZnO.

By including the doping impurities of Se/S, the neutral bonding defects are unstable with respect to lattice distortion which induces the valance alteration pairs (VAP) consisting of negatively charged singly bonded Se/S and positively charged triply bonded Se/S. If these same bonding states occurred in S/Se-doped a-Si:H, both donors and acceptors would be present in the same film thus making the properties of these films similar to boron-phosphorous[120] compensated a-Si:H.

2.3 Electrode preparation for electrical properties

Aluminium contacts of approximately 100 nm in thickness were deposited on the films in a coplanar configuration by thermal evaporator in a vacuum (1×10^{-5} torr). The samples were taken out from the vacuum chamber after 2 h of evaporation. The contacts were further verified for their Ohmic nature. Then the samples were loaded in a specially designed vacuum cryostat. A schematic illustration of the cryostat[142] is shown in Fig. 3.

Initially the films were annealed at 200°C in a vacuum cryostat to remove surface adsorption and metastable defects in the Se and S-doped a-Si:H thin films. The samples were then cooled slowly (1-2°C/min) to room temperature. A constant *dc* voltage from a highly stabilized power supply was applied across the samples and the current was

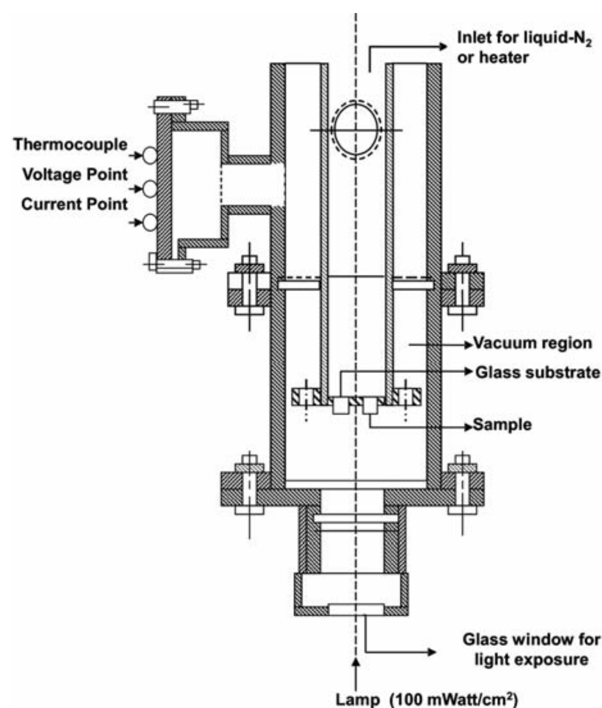

Fig. 3 — Schematic illustration for the cryostat

measured. The dark conductivity was measured once again upon warming. The measurements of conductivity variation were carried out in vacuum[106,108] in the temperature range 27-200°C at the rate of heating of 2-3°C/min. The photoconductivity was measured by illuminating the white light of a tungsten halogen lamp of intensity of 100 mWatt/cm^2. The lamp was calibrated using a standard detector (Hamamatsu S. 2281, Photodiode), in a vacuum in the temperature range 27-200°C. Intensity dependent on photoconductivity and persistent photoconductivity were also measured at room temperature, using a series of optical density filters[105]. Schematic illustrations for dark and photoconductivity measurements of thin films are shown in Fig. 4(a and (b). The value of the dark conductivity[109,143] was calculated from the relation:

$$\sigma = \frac{i \times L}{V \times t \times w} \ \Omega^{-1}\,\text{cm}^{-1} \qquad \ldots(1)$$

where L is the distance between the electrodes in cm, t is the thickness of the film in cm, w is the width of the film in cm, V is the applied voltage in volts (V) and i is the measured current in amperes (amp). The voltmeter and ammeter (Kaitheley) were connected as shown in Fig. 4. The details of the samples used for the experimental study of the electrical properties are given in Table 2.

2.4 Annealing effect on optical and electrical properties

After the deposition of Se-and S-doped a-SI:H thin films, all the samples were taken out of the deposition chamber and annealed in a microprocessor controlled furnace at temperatures in the range 100°-500°C in a vacuum (~1×10^{-6} torr) for an hour. The transmittance responses of these samples were measured after each annealing. The optical properties (bandgap, absorption coefficient, refractive indices etc.) were determined from the transmission spectra and compared with as-grown samples[109]. For conductivity measurements, all the procedures were used as mentioned above[143]. The band gap of a-Si:H can be varied from 1.7 to 2.0 eV by varying S and Se concentrations. The bandgap of Se and S-doped a-Si:H thin films was observed to be the highest at an annealing temperature of 300°C for both types of film and for all doping concentrations. Compared for a particular dopant concentration (or called impurities concentrations) of a gas ratio of H_2Se/SiH_4 and H_2S/SiH_4 =1×10^{-4} at an annealing temperature of 300°C, the bandgap was observed to be 1.85 eV in a-Si,Se:H films and 1.97 eV in a-Si,S:H films, respectively[121,144].

3 Optical Properties

Various methods have been used to determine the optical parameters of hydrogenated amorphous silicon thin films. These methods are classified into two groups: the first depends on the transmission or reflectance measurements[145], while the other comprises interferometric methods with two and multiple beam interferometry[146], and prism coupling technique[147]. For optoelectronic devices, an accurate determination of the optical constants, such as bandgap, absorption coefficient, refractive index, extinction coefficient with doping concentration and wavelength of semiconductor thin films, are important to precisely model their spectral response. The optical properties of S and Se alloyed hydrogenated amorphous silicon thin films (a-Si,S:H and a-Si,Se:H) have been reviewed and compared with other dopants.

3.1 Absorption coefficient

The absorption coefficient, α, can be calculated with an accuracy of ±2% in the weak and medium absorption regions, using the relation[148-150].

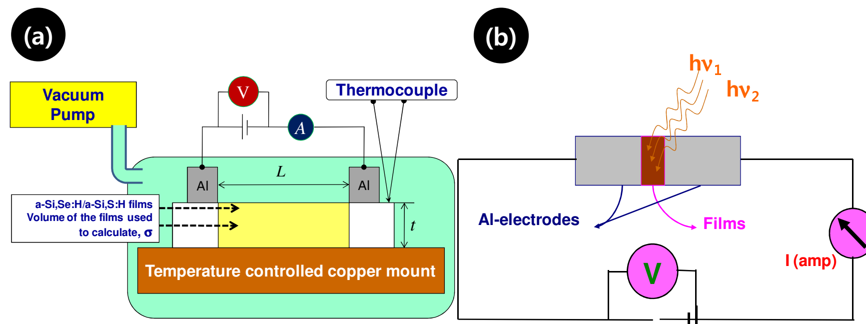

Fig. 4 — Schematic illustration for conductivity measurement setups of Se and S-doped a-Si:H thin films for (a) dark conductivity and (b) photoconductivity

$$\alpha = (1/d).[\ln(1/T)]$$

where d is the thickness of the films and T is the transmittance. The optimization procedure minimized differences between the experimental and theoretical transmittance in the broad spectral region including the region in the vicinity of the absorption edge[151], and the Tauc-Lorentz dispersion model for refractive index and extinction coefficient[152] that is currently employed for the parameterization of the spectral optical properties of amorphous materials[153].

3.2 Bandgap

The optical bandgap is one of the optical parameters that can be measured by using optical techniques based on transmission and reflection, for example Tauc's plot. A Tauc's plot is one of the methods to determine the optical band gap in semiconductors[108,109,154-159]. Other methods can be used to evaluate the bandgap of the materials, for example, ellipsometry[37], and the electrical energy gap method[160] (it can be measured under operation in an integrated device for many devices, for example lasers and solar cells). Tauc's relation is:

$$\alpha = B / h\nu\,(h\nu - E_g)^{\gamma} \qquad \ldots(2)$$

where B is a constant, E_g the optical bandgap energy, $h\nu$ the photon energy and γ depends on electronic transitions in k-space, and takes the values 1/2 for direct and 2 for indirect bandgap. The square root of the product of the absorption coefficient and photon energy $(\alpha h\nu)^{1/2}$ is plotted versus photon energy ($h\nu$). The curve should have a section of straight line. If extended to the x-axis, the x-intercept of this line gives the optical band gap. Fig. 5 shows the extensions of the intercepts on the x-axis to determine the value of the bandgap. As seen, the bandgap of a-Si, Se:H is lower than that for the case of a-Si, S:H for the same dopant concentration. This is due to the large binding energy of Si-S bond[161] (148 k cal/mol), as compared[121] to that of Si-Se (127 k cal/mol) and Si-Si bond (76 k cal/mol).

3.3 Refractive Indices

In the optical sciences, the refractive index is the most fundamental parameter in an optical medium. The refractive index determines the refraction and reflection occurring at the boundary between two media. In modern semiconductor materials, silicon is the most interesting material as a detector, reflector or absorber, where its refractive index is of primary importance. The refractive index of Se and S-doped a-Si:H thin films were determined by using transmission spectra in the weak and medium absorption region using the following expressions[107,109]:

$$n = \left[N + \left(N^2 - s^2 \right)^{1/2} \right]^{1/2}$$

where

$$N = \frac{s^2+1}{2} + 2s\frac{T_M - T_m}{T_M T_m} \qquad \ldots(3)$$

where s is the refractive index of the substrate, and T_M and T_m are the maxima and minima of the fringes of transmission spectra as shown in Fig 2. The refractive index was determined to an accuracy of 1-2%. Dusane *et al*[112]. have shown that in *p*-doped a-Si:H, bond angle deviation increases sharply with increasing dopant concentrations. Increase in bond angle deviations causes internal strain in an amorphous network. The decrease in refractive index for Se- and S-doped a-Si:H might be due to the increase in internal strain, as in the case of *p*-doped a-Si:H film. The refractive index of a semiconductor has a strong dependence on the value of the bandgap: the higher the bandgap, the smaller the refractive index[162,163]. The refractive index, n (at a particular wavelength, λ=750 nm) as a function of bandgap for various semiconductors[107] is shown in Fig. 6. It is interesting to note that the values of refractive index for our samples a-Si,Se:H and a-Si,S:H lay almost on the

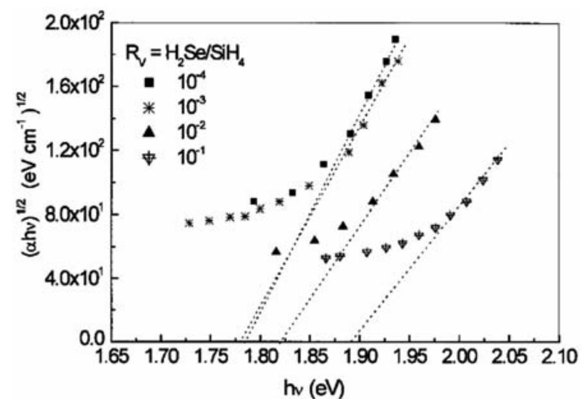

Fig. 5 — Typical plot of bandgap versus energy by Tauc's plot for Se-doped a-Si:H thin films. Reproduced with permission from the authors of Ref. 107; Copyright 2002, WILEY-VCH Verlag GmbH & Co. KGaA

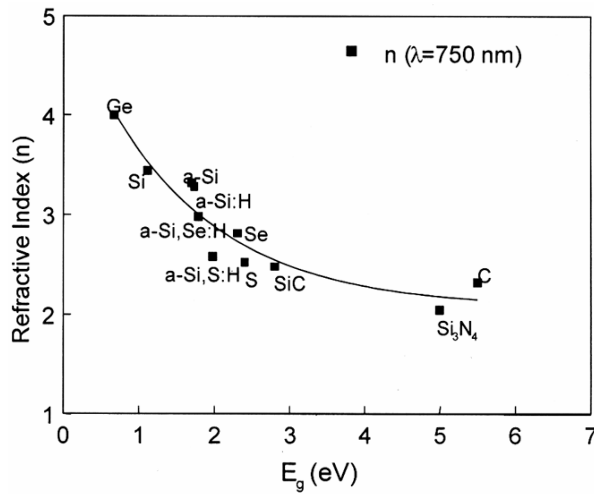

Fig. 6 — Refractive index versus bandgap for various semiconductor materials. Reproduced with permission from the authors of Ref. 107; Copyright 2002, WILEY-VCH Verlag GmbH & Co. KGaA

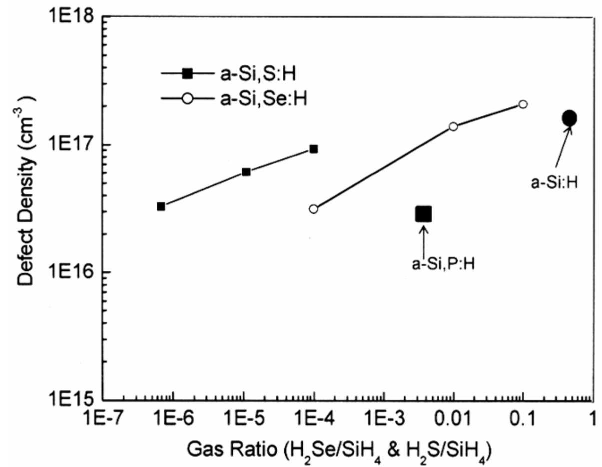

Fig. 7 — Defect density of intrinsic and doped a-Si:H thin films

Table 3 — Comparison of optical constants: absorption coefficient (α), bandgap (E_g) and Refractive index (n) for similar doped a-Si, Se:H and a-Si,S:H films and other dopants in a-Si:H

S. No.	Films	Absorption coeff. α (eV)	Bandgap E_g (eV)	Refractive Index (n)
1.	a-Si:H	>1000	1.70	4.30
2.	a-Si,S:H	2037.80	1.79	2.58
2.	a-Si,Se:H	3527.35	1.96	2.98
3.	a-Si,P:H		1.81	
4.	a-Si,C:H		1.95	
5.	a-Si,Ge:H		1.52	

curve. Table 3 presents the values of optical constants, such as absorption coefficients, α, refractive index, n, and bandgap, E_g. The optical constants of intrinsic, Se-, S-, P- and B-doped a-Si:H have been compared.

3.4 Defect density of a-Si:H

Hydrogenated amorphous silicon is a disordered semiconductor, whose optoelectronic properties are governed by the large number of defects present in its atomic structure. The silicon atoms have the same number of neighbours and on average, the same bond lengths and bond angles. One can represent the disorder by the atom pair distribution function, which is the probability of finding an atom at a distance r from another atom.

The defect density (N_d) was obtained from the magnitude of the sub-gap absorption shoulder, using the same conversion factor[164] as that used for a-Si:H. Figure 7 shows the defect density of intrinsic and Se-, S-, *p*-doped a-SiH films. Sharma *et al*[107]. investigated the linear rise of N_d from about 3.3×10^{16} to 9.3×10^{16} as the doping gas ratio (H_2S/SiH_4) increased from 6.8×10^{-7} to 1.0×10^{-4} for S-doped films, and from 3.2×10^{16} to 2.1×10^{17} as the doping gas ratio (H_2Se/SiH_4) increased from 1.0×10^{-4} to 1.0×10^{-1} for Se-doped films. It is evident that the defect density in Se-doped films was smaller than that for S-doped films for the same dopant gas ratio ($R_V = 10^{-4}$). This also explains the observed higher conductivity of Se-doped films, as compared to S-doped films. The defect density[165] was compared with intrinsic and *p*-doped a-Si:H films and the comparisons are shown in Fig. 7.

4 Conductivity

The conductivity is a macroscopic quantity, which represents an average property of the carriers as they move from one site to another. The carriers (electrons or holes) in extended states are conducting, and in localized states are non-conducting. The conduction mechanism involves the transfer rate, scattering and trapping processes, as well as the appropriate average over the distribution of states. The conductivity is the product of the carrier density and the carrier mobility[166]:

$$\sigma = ne\mu \qquad \ldots(4)$$

The total conductivity at a finite temperature can be written as:

$$\sigma = \int \sigma_E \frac{\partial f(E)}{\partial E} dE \quad \ldots(5)$$

where σ_E is the conductivity for states with energy E and $f(E,T)$ in the Fermi-Dirac distribution function is given by:

$$f(E) = \frac{1}{1+\exp\left[(E-E_F)/kT\right]} \quad \ldots(6)$$

The integral contains contributions from electron transport above Fermi level (E_F) and hole transport below E_F. Using the relationship:

$$\frac{\partial f(E)}{\partial E} = -f(E)\frac{\left[1-f(E)\right]}{kT} \quad \ldots(7)$$

σ, can be written as:

$$\sigma = e\int N(E)\mu(E) f(E)\left[1-f(E)\right] dE$$

where, $\mu(E)$ and $N(E)$ are the mobility and density of states, respectively at an energy E.

4.1 Thermal Equilibration Temperature (T_E) and Barrier Energy (E_B)

The equilibration of the material represents a considerable simplification on our understanding of a-Si:H, because thermodynamic models can be used to predict the electronic properties. It may seem surprising to apply thermal equilibrium concepts to amorphous silicon, because the amorphous phase of a solid is not the equilibrium phase. However, a subset of bonding states may be in equilibrium, even if the structure as a whole is not in its lowest energy state. The attainment of equilibrium is prevented by bonding constraints on the atomic structure. Equilibrium is calculated from the formation energies of the various states by minimizing the free energy. The kinetics are described by a relaxation time, τ_R, required for the structure to overcome the bonding constraints. τ_R is associated with an energy barrier, E_B, which arises from the bonding energies, and is shown in Fig. 8 (c) by a configurational coordinate diagram. The lower energy well may represent the fully coordinated network, and the higher energy well dangling bond defects. The energy difference is the defect formation energy, U_d, and determines the equilibrium defect density. The equilibration time, on the other hand, is given by the barrier height[166]:

$$\tau_R = \omega_o^{-1} \exp\left(\frac{E_B}{kT}\right) \quad \ldots(8)$$

A larger energy barrier obviously requires a higher temperature to achieve equilibrium in a fixed time. The formation energy U and the barrier energy E_B are often of very different magnitudes. Figure 8(a) shows the energy barrier, which exhibits high temperature equilibrium and a low temperature frozen state. The temperature, T_E, at which freezing occurs was calculated from Eq. (1) by equating the cooling rate with $dT/d\tau_R$:

$$T_E \ln\left(\frac{\omega_o k T_E^2}{R_C E_B}\right) = \frac{E_B}{k} \quad \ldots(9)$$

where R_C is the cooling rate. An approximate solution to Eq. (2) for a freezing temperature in the vicinity of 500K is:

$$k T_E = \frac{E_B}{(30 - \ln R_C)} \quad \ldots(10)$$

Below T_E, the equilibration time is observed as a slow relaxation of the structure towards the equilibrium state[107,166]. Figure 8(b) shows the typical Arrhenius plot of Se-doped a-Si:H films for the highest and lowest dopant concentrations. It is seen from Fig. 8(b) that the conductivity is a function of thermal history i.e. rate of cooling of the samples below a certain temperature, known as the thermal equilibration temperature (T_E). The conductivity is found to be activated above T_E. It is observed from Fig. 8(b) that the room temperature conductivity varies by an order with the cooling rates. The conductivity was enhanced by quenching the samples. The barrier energy, E_B as a function of cooling rate, R_C is calculated by Eq. (3). The variations of E_B versus doping ratio for different Se and S doping concentration and cooling rates (slow and rapid cooling) are shown in Fig. 8(d). This shows that the barrier energy for slow cooled films is slightly higher than for rapid cooled films.

4.2 Mayer-Neldel rule

The Meyer-Neldel Rule (MNR) is an exponential relation between the activation energy and the pre-exponential factor, for the measurement of conductivity with temperature[106,167]. It has been observed in a large range of materials from amorphous/crystalline semiconductors[106,168,169], to organic solids[170-173]. Thermally activated conductivity, σ, via extended states in a-Si:H can be described experimentally by the Arrhenius equation:

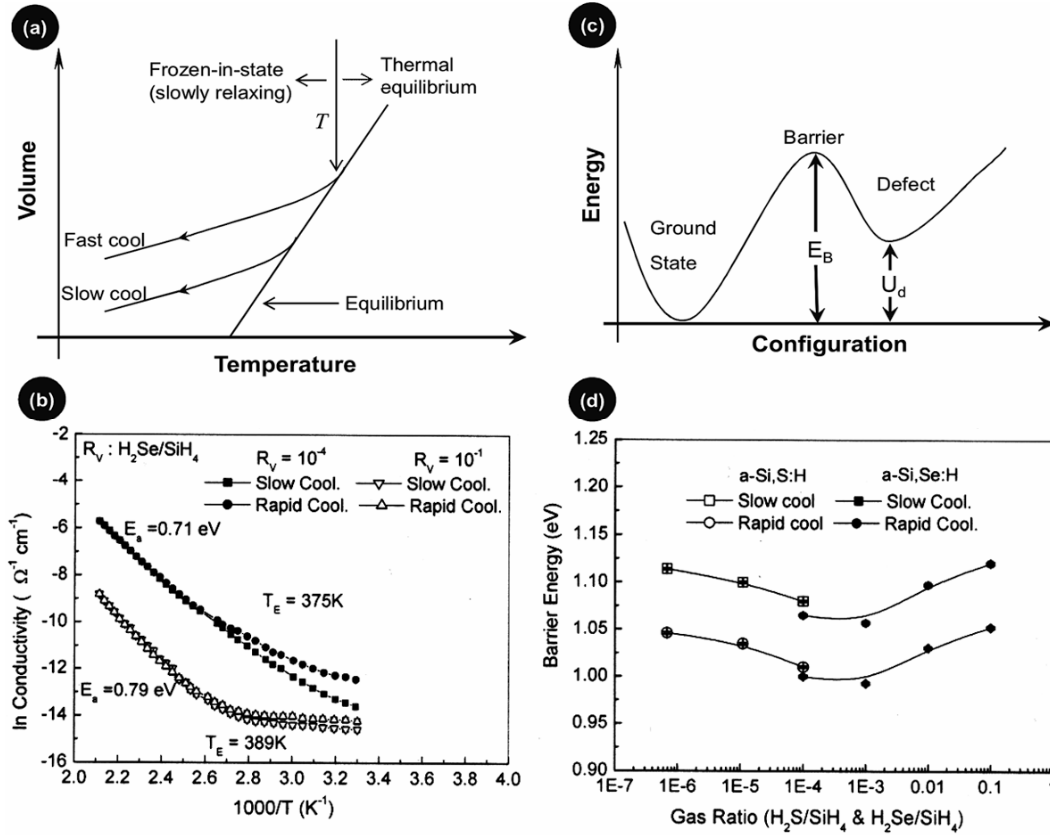

Fig. 8 — (a) Schematic illustration of thermal equilibrium model, (b) Arrhenius plots for slow and rapid cooling of the systems, (c) schematic illustration for energy barrier model, and (d) barrier energy versus doping gas ratios of Se and S-doped a-Si:H thin films. Figs. 8(b) and (d): reproduced with permission from the authors of ref. 108; Copyright 2003, Taylor & Francis Ltd

$$\sigma = \sigma_o \exp\left(\frac{-E_a}{kT}\right) \quad ...(11)$$

where σ_o is the conductivity prefactor, E_a the activation energy, k the Boltzmann constant and T is the absolute temperature. The Meyer-Neldel Rule proposed that[167]:

$$\sigma_o = \sigma_{oo} \exp\left(\frac{E_a}{E_{MN}}\right) \quad ...(12)$$

where σ_{oo} and $1/E_{MN}$ are the MNR prefactor and the MNR slope, respectively[174,175]. The observed values for the characteristic energy E_{MN} in various materials and processes[175] have been measured to be between 25 and 100 meV. A combination of Eqs (1 and 2) gives a general expression for σ_o as:

$$\sigma = \sigma_{oo} \exp\left[\left(\frac{1}{E_{MN}} - \frac{1}{kT}\right) E_a\right] \quad ...(13)$$

This implies a single crossing point for the different activation energies at an isokinetic temperature T_{MN} determined by the MNR, $T_{MN}=E_{MN}/k$. At this temperature, σ is independent of the activation energy. Different models have been applied for explaining the Meyer-Neldel rule, which includes the density of states (DOS) model, which is related to a systematic change in DOS in the mobility gap and statistical shift of Fermi energy $E_F(T)$, and is responsible for the application[176-178]of MNR. In a plot of ln(σ) versus inverse temperature, the curves of different doped samples should show one common intersection at T_{MN}. It is found that the Arrhenius plot deviates from a linear behaviour in the form of continuous bending[176-181]. The origin of the non-linearity varies from experiment to experiment. Yoon and Lee[182] argued that statistical shift of Fermi level can cause the bending. The conductivity due to variable range hopping of electrons between localized states as proposed by Mott[183], is given by:

$$\sigma = \sigma_{ho}\, e^{-\left(\frac{T_o}{T}\right)^{\frac{1}{4}}} \qquad \ldots(14)$$

where σ_{ho} and T_a have been given by Hill *et al.*, as:

$$\sigma_{ho} = \left[\frac{3e^2 \nu_{ph}}{(8\pi k)^{\frac{1}{2}}}\right] \times \left[\frac{\lambda\alpha^3}{N(E_F)}\right]^{\frac{1}{2}}, \qquad \ldots(15)$$

$$T_o = \frac{\lambda\alpha^3}{k\,N(E_F)} \qquad \ldots(16)$$

where v_{ph} is the photon frequency at Debye temperature ($\sim 10^{+13}$ s^{-1}), k Boltzmann's constant, $N(E_F)$ is the density localized states for electrons, α the range of the wave function localized state and λ is a dimensionless constant (~16). Several researchers have found[184,185] a linear dependence of ln(σ) versus $T^{-1/4}$ at low temperature (300-370 K), indicating that variable range hopping conduction of localized electrons in Se and S-doped a-Si:H thin films occurs in this range of temperature. Two other Mott's parameters, hopping distance R, and the average hopping energy W, can also be evaluated using the relation as:

$$R = \left[\frac{9}{8\pi\alpha k T\, N(E_F)}\right]^{\frac{1}{4}} \qquad \ldots(17)$$

$$W = \left(\frac{3}{4\pi R^3\, N(E_F)}\right) \qquad \ldots(18)$$

A good linearity between ln($\sigma T^{1/2}$) and $T^{-1/4}$ plots confirms Mott's equation for any given data, and for VRH to be the Mott's constants, $\alpha R > 1$ and $W > kT$ must be fulfilled.

The electrical conductivities of Se and S-doped a-Si:H thin films have been analyzed as a function of temperature and dopant concentration. The MNR has been found to be satisfied for thermally activated conductivities in Se and S doped a-Si:H films. It is also observed that there exists a strong correlation between the MN conductivity prefactor and activation energy. The origin of this correlation can be attributed to the statistical shift of the Fermi energy in band gap. The characteristic energy E_{MN} (= kT_{MN}) for Se and S-doped a-Si:H films is 54 meV and 50 meV, respectively. This corresponds to a characteristic temperature of 616 and 591 K, respectively, where the conductivity data becomes independent of dopant concentrations[106]. The conductivity due to variable range hopping of electrons between localized states at low temperature has been observed for all compositions of the films and is described in Table 4.

5 Photoconductivity

Photoconductivity (PC) plays a dominant role to study the hydrogenated amorphous silicon (a-Si:H), because of optoelectronic device applications[142,186]. This is the increase in electrical conductivity of a photosensitive material when it is exposed to electromagnetic radiation. This occurs when carriers are optically excited from non-conducting to conducting states. Certain crystalline/amorphous semiconductors, such as silicon (Si), germanium (Ge), lead sulphide (PbS), and cadmium sulphide (CdS) and the related semi-metal selenium (Se), are strongly photoconductive. The study of photoconductivity in hydrogenated amorphous silicon (a-Si:H) is a valuable tool for achieving a good understanding of the recombination processes and for obtaining basic information on the localized states that control the recombination of free carriers in this material. The photoconductive effect is the result of several processes whereby photons cause electrons to be ejected from the valence band and injected into the conduction band as shown in Fig. 9. The parabolic curves are shown in the schematic illustration which represent the conduction band (E_C), metastable band (E_M) and valance band (E_V). During illumination, the electrons are excited, and reach the conduction band edge, as represented by the optical absorption (ΔE_{Opt}) in the diagram.

The numbers of conduction electrons and holes increase simultaneously, and the effect is called intrinsic photoconductivity. When electrons from a filled band are injected into vacant impurity levels, the number of holes increases; this effect is referred to

Table 4 — Mott's parameters for Se and S-doped hydrogenated amorphous silicon films (Ref.2)

Gas Ratio	Sample	$N(E_F)$	α	R	W
	6.8×10^{-7}	1.248×10^{27}	3.510×10^{10}	7.494×10^{-10}	0.454
H_2S/SiH_4	1.1×10^{-5}	1.965×10^{22}	7.364×10^{8}	3.127×10^{-8}	0.397
	1.0×10^{-4}	6.508×10^{20}	2.365×10^{8}	9.738×10^{-8}	0.397
	1.0×10^{-4}	2.217×10^{21}	3.539×10^{8}	6.480×10^{-8}	0.396
H_2S/SiH_4	1.0×10^{-3}	2.344×10^{13}	7.768×10^{5}	2.953×10^{-5}	0.396
	1.0×10^{-2}	6.596×10^{19}	7.044×10^{7}	2.336×10^{-7}	0.284
	1.0×10^{-1}	0	7.342×10^{-15}	6.990×10^{14}	0.089

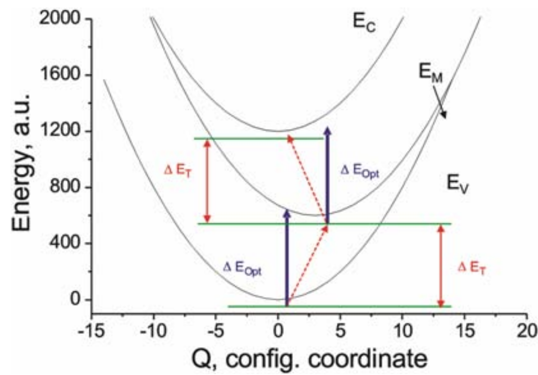

Fig. 9 — Schematic configuration coordinate diagram for the energy bands, ground state and excited states

as p-type extrinsic photoconductivity. If electrons are ejected from impurity levels and injected into the conduction band, the effect is known as n-type extrinsic photoconductivity. The combined excitation of intrinsic and extrinsic photoconductivity is also possible. Such combined excitation is called exciton-induced photoconductivity, and occurs when the excitation of intrinsic photoconductivity leads, as a result of the ensuing processes of carrier trapping to the occupation of impurity centers, and consequently to the occurrence of extrinsic photoconductivity.

5.1 Steady-State Photoconductivity

Steady state photoconductivity measurements give information about the nature of defects, mobility-lifetime products and the transport and recombination kinetics of photogenerated carriers. Since the states between quasi-Fermi levels act predominantly as recombination centres, steady state photoconductivity is sensitive to both the density and the nature of these states. Steady state photoconductivity involves three mechanisms: (i) Absorption of photons by the material, and generation of free electron-hole pairs. (ii) Separation of electrons and holes, and transport of the mobile photo-generated carriers. (iii) Recombination of excess free electrons and holes via recombination centers, which are located between the quasi Fermi levels for electrons and holes, respectively[186-191].

Under the action of absorbed light, the densities of charge carrier electrons (n) and holes (p) increase, as compared with their values at thermal equilibrium. If n_o and p_o denote the equilibrium densities of electrons and holes, then, in the presence of photo-excitation, the bulk conductivity contains two components: the dark conductivity (for an n-type sample) and μ_n, is the electron mobility in the conduction band (extended states for electrons).

$$\sigma=\sigma_o+\Delta\sigma \text{, where, } \sigma_o = ne\mu_n \quad \ldots(19)$$

The excess conductivity or photoconductivity can be expressed as:

$$\Delta\sigma = e(\Delta n\mu_n + \Delta p\mu_p) \quad \ldots(20)$$

where Δn is the additional photo-excited electron density, with charge e and mobility μ_n. Similarly, Δp is the additional photo-excited hole density with mobility μ_p. At low temperature, the value may be considerably higher than the equilibrium value.

5.1.1 Temperature dependent photoconductivity

The exposure of intrinsic and extrinsic a-Si:H films to white light at an intensity of about 100 mW cm^{-2} for several hours (light soaking) induces changes in the temperature dependence of the photo-conductivity[105,192-194]. The actual photoconductivity (σ_{ph}) of a-Si:H thin films at room temperature can be calculated by this relation:

$$\sigma_{ph} = \sigma_{ill} - \sigma_{dc} \quad \ldots(21)$$

where $\sigma_{ill\rightarrow}$ conductivity measured during illumination, $\sigma_{dc\rightarrow}$ conductivity measured in darkness, which can be measured directly by using the relation given in Eq. (21). The parameters used for calculation are shown in Fig. 4.

The temperature dependence of photoconductivity of a-Si:H thin films for the conduction mechanism is assumed to be:

$$\sigma = \sigma_o \exp\left(-\frac{E_a}{kT}\right) \quad \ldots(22)$$

where E_a is the temperature independent activation energy and σ_o is the pre-exponential factor for conductivity. Typical temperature dependence of photoconductivity of a-Si,Se:H and a-Si,S:H thin films[105] is shown in Fig. 10.

The σ_{ph} of S-doped a-Si:H films was lower than the σ_{ph} of Se-doped a-Si:H films as compared at a similar dopant concentration (H_2Se/SiH_4 and H_2S/SiH_4 = 1 × 10^{-4}). At room temperature, the σ_{ph} was much higher than the dark conductivity at each of the dopant concentrations, due to light soaking. The light soaking introduced effective recombination centers other than the normal dangling bond (DB), with relatively low concentrations. The recombination induced weak bond breaking with successive

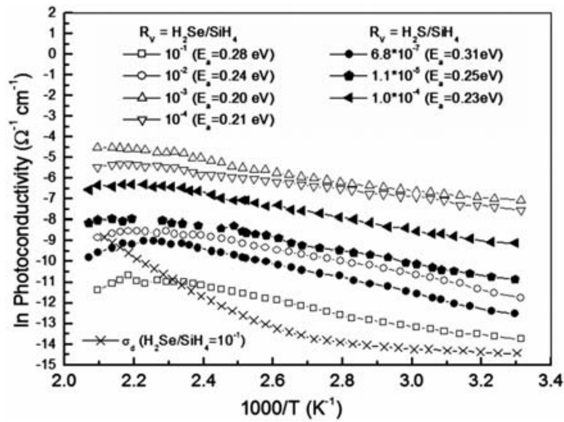

Fig. 10 — Photoconductivity versus inverse temperature of Se-doped for the gas ratio from $H_2Se/SiH_4=10^{-4}$ to 10^{-1}, and S-doped for the gas ratio from $H_2S/SiH_4=6.8\times10^{-7}$ to 1.0×10^{-4}, and the dark conductivity for Se-doped, $H_2Se/SiH_4 = 10^{-1}$, a-Si:H thin films. Reproduced with permission from the authors of ref. 105; Copyright 2009, Elsevier

hydrogen mediated separation of the DB. It is clear that the DB separation process becomes less effective at lower temperatures. The temperature dependence of σ_{ph} for Se and S-doped a-Si:H films is also similar to that observed for *p*-doped films[195]. The activation energy in photoconduction decreased from 0.31 to 0.23 eV, as the gas ratio (H_2S/SiH_4) of S-doped films increased from 6.8×10^{-7} to 1.0×10^{-4}. The activation energy decreased from 0.21 to 0.20 eV, as the gas ratio (H_2Se/SiH_4) of Se-doped films increased from 10^{-4} to 10^{-3}; and then increased to 0.28 eV, as the gas ratio increased to 10^{-1}. Thus the σ_{ph} is found to be activated in the temperature range 27°-200°C. For higher dopant concentration, $H_2Se/SiH_4 = 10^{-1}$, σ_{ph} was observed to be lower than the dark conductivity for a temperature greater than 170°C. As the Fermi-level in *n*-type a-Si:H is located above the position of D_o states (neutral dangling bonds, which is equal to $N_o \approx n_t + N_o^o$, where N_o^o is the concentration of D_o in the dark and n_t is the concentration of electron trapped by the conduction band tail states[196,197], which seems to be determined by N_o^o), N_o^o would be increased with respect to temperature and correspondingly σ_{ph} would be decreased.

5.1.2 Intensity dependence of photoconductivity

Intensity dependence of photoconductivity is one of the properties of the steady-state photoconductivity of semiconductors and is dependent on the intensity of the illumination. Intensity dependence of photoconductivity[105,186,198], σ_{ph}, is directly related to the intensity of illumination, *F*, as given below:

$$\sigma_{ph} \propto F^{\gamma} \qquad \ldots(23)$$

where the exponent γ is equal to either 1, corresponding to monomolecular recombination mechanisms, or 0.5, corresponding to bimolecular recombination. However, as in many amorphous semiconductors, particularly a-Si:H, γ is a constant and intermediate values of the exponent γ are found i.e. $0.5 \leq \gamma \leq 1$. It is defined differentially as:

$$\gamma = \frac{d\left(\ln \sigma_{ph}\right)}{d\left(\ln G\right)} \qquad \ldots(24)$$

The dependence of the photoconductivity on the excitation intensity is a well-known fact in crystalline solids[186]. Consider a simple model of a semiconductor with only one type of recombination center. If an excess electron density Δn is established by light excitation, then, assuming the material to be intrinsic ($n_o=p_o$) and that charge neutrality exists ($\Delta n = \Delta p$), one has:

$$\frac{d\left(\Delta n\right)}{dt} = G - \left[C_n\, N_r \left(n_o + \Delta n\right) - C_n\, n_o^2\right] \qquad \ldots(25)$$

where n_o is the density of thermal carriers available to recombine with the excess carriers, C_n the capture coefficient and N_r is the concentration of the recombination centers. In the steady state, $d(\Delta n)/dt = 0$, and

$$G = C_n \left(\Delta n^2 + 2 n_o\, \Delta n\right) \qquad \ldots(26)$$

This relation gives a direct insight into the dependence of Δn on the generation rate, and consequently on the light intensity, which is proportional to *G*. In the regime $n_o >> \Delta n$ (this condition is satisfied if the resistivity is small or for low illumination intensities),

$$\Delta n = \frac{G}{2 C_n\, n_o} \; \left(\text{monomolecular}\right) \qquad \ldots(27)$$

and the photocurrent varies linearly with the excitation intensity. When $n_o << \Delta n$,

$$\Delta n = \left(\frac{G}{C_n}\right)^{1/2} \quad (\text{bimolecular}) \qquad \ldots(28)$$

and the photocurrent is proportional to the square root of the light intensity. This case applies to low temperature and high excitation, when the photoconductivity exceeds the dark conductivity.

The typical intensity[105] dependence of σ_{ph} of Se and S-doped a-Si:H thin films is shown in Fig. 11. The σ_{ph} as a function of the intensity of the exciting light is very similar to that commonly observed in a-Si:H, which is observed to obey a power-law relation, Eq. (6). The value of γ is found to be $\approx$ 0.75 for the gas ratio H_2Se/SiH_4 = 10^{-4} to 10^{-3}, indicating a mixture of monomolecular and bimolecular recombination mechanisms and from the gas ratio $H_2Se/SiH_4=10^{-3}$ to 10^{-1}, decreases to 0.51, indicating the bimolecular mechanism. This is consistent with the results that heavily doped samples are more resistive, and so bimolecular recombination is predominant in these films. For the S-doped films, γ has been found to be $\approx$ 0.73 as the gas ratio (H_2S/SiH_4) increased from 6.8×10^{-7} to 1.0×10^{-4}, indicating a mixture of monomolecular and bimolecular recombination mechanism. The illumination was performed at room temperature, with IR-filtered white light whose intensity was 100 m-watt/cm^2. The photosensitivity (σ_{ph}/σ_d) of a-Si,Se:H films decreased as the gas ratio H_2Se/SiH_4 increased from 10^{-4} to 10^{-1}. The photosensitivity of a-Si,S:H films increased as the gas ratio H_2S/SiH_4 increased from 6.8×10^{-7} to 1.0×10^{-4}.

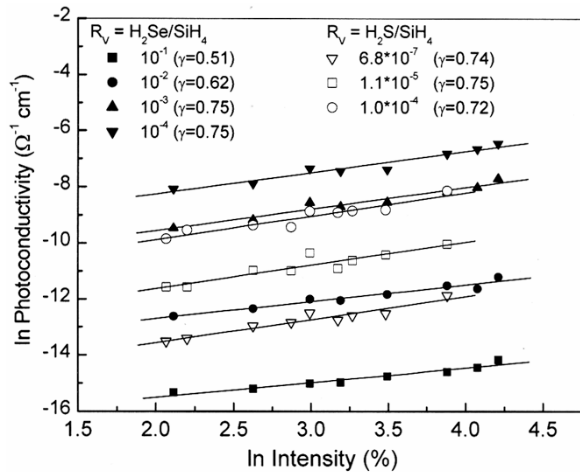

Fig. 11 — Intensity dependence of photoconductivity of Se- and S-doped a-Si:H thin films for various dopant concentrations. Reproduced with permission from the authors of Ref. 105; Copyright 2009, Elsevier

5.2 Transient Photoconductivity

The transient photoconductivity is determined by using time dependence of the photocurrent, which is the carrier excitation of a short pulse of illumination in samples with a coplanar electrode configuration. There are three generic aspects of transient photoconductivity: carrier photo generation, carrier mobility and carrier recombination processes. This is also well suited for lifetime analysis of amorphous/crystalline semiconductor material, since *p-n* junction formation is not required[199-202]. The transient photoconductivity of polymers or organic semiconductors implies the existence of a well-defined internal field: carrier sweep-out, which is proportional to the magnitude of the internal field and limited by the carrier mobility[203-205].

6 Persistent Photoconductivity

Persistent photoconductivity (PPC) is a photo-induced conductivity or excess conductivity in semiconductor materials, which persists for a period after the termination of the illumination. It can also be defined in terms of the defect clusters developed during illumination in semiconductors, which may cause persistent photoconductivity. This can provide valuable information about the metastability of impurities, the mechanisms for carrier storage and relaxation, and the transport properties in disordered systems. It is important for electronic and photonic device applications to find out the cause of PPC in a semiconductor system[206,207].

6.1 Observation of persistent photoconductivity

There has been a considerable amount of experimental and theoretical efforts directed towards the understanding of persistent photoconductivity, which has been observed in a variety of semiconductors, for example, hydrogenated amorphous silicon[208-210] (a-Si:H), rough silicon membrane[211] nanostructured[212-214] ZnO, III-V compound semiconductors[215-217], $SrTiO_3/LaAlO_3$ heterostructures[218], chalcognides[219,220], quaternary alloys[221-223], and so on. The PPC has been investigated by various models, among which the Large-Lattice-Relaxation model, Macroscopic Barrier model, and Random Local Potential Fluctuations model are the most well-known for the explanation of PPC in semiconductor thin films[224,225]. The large lattice relaxation model involves photoexcitation of electrons from deep-level traps (DX centers), which endure a lattice relaxation, to shallow effective-mass states[226,227]. An electron-capture barrier is created by

lattice relaxation, preventing recapture of electrons by DX centers. At low temperatures, thermal energy is not enough to defeat the capture barrier, and the electrons remain in the shallow states, resulting in PPC. Another model for PPC is the spatial separation of photo-excited electrons and holes by macroscopic potential barriers, due to band bending at surfaces or interfaces[228]. The last model to describe PPC is the random local-potential fluctuation (RLPF) model. In this model, the spatial separation between photo-excited charge carriers by random local-potential fluctuations induced by compositional fluctuations[229] is responsible for PPC.

6.2 Persistent photoconductivity effect

The PPC effect has been observed in undoped, *n*-type and *p*-type a-Si:H thin films, as well as in other materials. Kakalios *et al*[230]. detected excess conductivity after a brief light exposure at room temperature. This effect might be attributed to the spatial separation of photo carriers by the *pn* junction fields, which was electronic or optical tuning, and is dependent on the magnitude of the internal electric fields. Choi *et al*[231]. verified that the PPC can disappear after annealing at 500°C, i.e. the deep traps defect can be removed completely. PPC creation could also be related to sample inhomogeneity. Hamed[99] explained the PPC effect in *p-n* multilayers of a-Si:H. The equilibrium Fermi level of the multilayers was observed closer to the conduction band in the depletion zones of the *n*-type regions, causing an increase in the conductance, due to the excess carrier concentrations generated by light, rather than to the field-separated photocarriers. The results indicated that the depletion zones of a multilayer, where the Fermi level lies closer to mid-gap, have a lower concentration of defects, and perhaps a higher doping efficiency, than the bulk or non-depleted zones.

Wang *et al*[95]. found a persistent photoconductivity (PPC) in a-Si,S:H films, whose effect on both the conductivity and photoconductivity is opposite to the Staebler-Wronski effect. Therefore, it was expected that the presence of the PPC effect might increase the stability of the materials and devices. Wang *et al*[232]. added S impurities to a-Si:H thin films, which increased the dark conductivity and decreased the activation energy. In the case of low dopant concentration (less than 10^{-3}), the photoconductivities are about 10^{-3} $\Omega^{-1}cm^{-1}$ under one-sun light intensities. Taylor[233] detected deleterious metastabilities, which were known loosely and collectively as the Staebler-Wronski effect by the addition of chalcogen elements (S and Se) into a-Si:H. S-and Se-doped a-Si:H films, which resulted in a decrease of the degradation of conductivity and photoconductivity. Mehra *et al*[120]. observed that the PPC at room temperature increased with increasing illumination. Photodegradation results indicated that a-Si,Se:H films would be more stable than a-Si,S:H films, as the compensation of the photodegradation due to PPC is larger in the case of Se-doped films. Sharma *et al*[105]. also investigated similar phenomena for both Se and S-doped a-Si:H. The typical Arrhenius plot of a-Si,Se:H films for the particular doping gas ratio $H_2Se/SiH_4 = 10^{-3}$ with different illumination time, showed that the conductivity increased and activation energy decreased as shown in Fig. 12.

7 Annealing of a-Si:H

The stability of amorphous silicon alloys with respect to heating and light soaking is of considerable scientific and technological interest[234-236]. Annealing and outgassing of a-Si:H appears to remove many of the defects and structures that are responsible for the low efficiencies and poor stability of amorphous silicon solar cells. Heating also reduces the hydrogen concentration of the films, and this could be a disadvantage for photovoltaic performance, unless the dangling bonds are also removed in the process, or by subsequent annealing[143]. These effects, therefore, require further investigation as a possible means of improving the performance of a-Si:H solar cells.

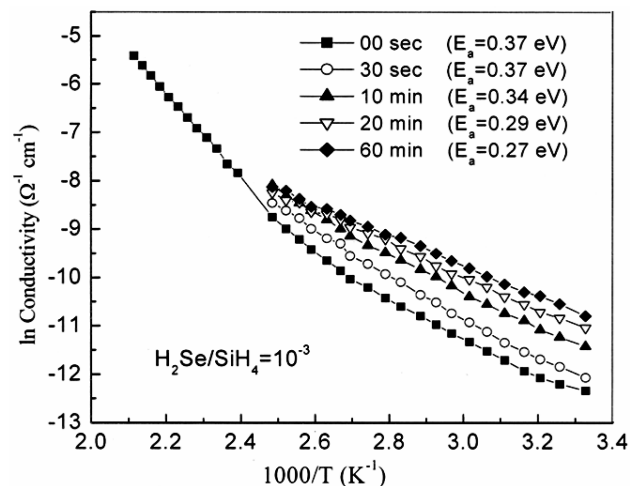

Fig. 12 — Typical Arrhenius plots for excess conductivity with various illumination times. Reproduced with permission from the authors of ref. 105; Copyright 2009, Elsevier

8 Conclusions and Future Prospects of Se and S-doped a-Si:H

The dopant concentration in silicon was observed to increase with increasing doping gas ratios in chamber during depositions. A smaller bandgap was observed in the case of the a-Si,Se:H films with a similar gas ratio, this may be because of larger binding energy of the Si-S bond than that of the Si-Se bond. The absorption coefficient and extinction coefficient are higher, in the case of Se-doped a-Si:H films. Therefore, better optoelectronic properties for Se-doped a-Si:H can be obtained for a lower doping concentration of Se, as compared to S-doped samples, which is a great advantage. The defect density in Se-doped films was smaller than that for S-doped films for the same dopant gas ratio.

The barrier energy for slow cooled films is slightly higher than for rapid cooled films. The MNR has been found to be satisfied for thermally activated conductivities in Se and S doped a-Si:H films. The origin of this correlation can be attributed to the statistical shift of the Fermi energy in band gap. The conductivity due to variable range hopping of electrons between localized states at low temperature has been observed for all compositions of the films.

Light incident on a-Si:H causes metastable Si dangling bond (DB) defects to form with the result of increased carrier trapping and decreased photoconductivity. Much theoretical and experimental effort has been put into understanding the SWE, but a comprehensive explanation has yet to be achieved. The photoconduction in hydrogenated amorphous silicon (a-Si:H) is sensitive to doping concentration such as chalcogens (Se and S). Doping can also have an effect on the temperature dependence of photoconductivity, as well as on *dc* dark conductivity. The photosensitivity of a-Si,Se:H films decreased as the gas ratio increased, while the photosensitivity of a-Si,S:H films increased as the gas ratio increased.

Remarkable progress and improvement in the optical and electrical properties of double donor (Se and S) hydrogenated amorphous silicon thin film should be considered as an alternative to wide band gap materials for the absorbing layers in optoelectronic devices. Values of the optical and electrical parameters are the highest achieved for a-Si,Se:H and a-Si,S:H thin films, as compared with pentavalent element-doped a-Si:H films. It is expected that during illumination, the excess electron will contribute in the conduction to the electron collecting electrode.

Acknowledgement

Appreciation is extended to Prof PC Taylor of the University of Utah, and K-N P Kumar of the University of Texas at Dallas for their initial inspiration and valuable discussion. This research was supported by the Leading Foreign Research Institute Recruitment Program through the National Research Foundation of Korea (NRF) funded by the Ministry of Education, Science and Technology (MEST) (Grant No. NRF-2013-044975).

References

1 (http://en.wikipedia.org/wiki/Silicon).
2 Abundances of the Elements in the Earth's Crust, Hyperphysics, Georgia State University, (http://hyperphysics.phy-astr.gsu.edu/hbase/tables/elabund.html).
3 Sze S M & Ng K K, *Physics of semiconductor devices, 3rd edition, Wiley*, © 2007.
4 Baker R J, "Circuit layout, Design and Simulation", *IEEE Press, Wiley-Interscience,* USA, © 2005.
5 King T J, Mcvittie J P, Saraswat K C & Pfiester J R, *IEEE Trans Electron Dev*, 41 (1994) 228.
6 Jeon T & Grischkwsky D, *Phys Rev B*, 78 (1997) 1106.
7 Roth T, Rosenits P, Diez S, Glunz S W, Macdonald D, Beljakowa S & Pens G, *J Appl Phys*, 102 (2007) 103716.
8 Scala R, Porrini M & Borionetti G, *Cryst Res Tech*, 46 (2011) 749.
9 Fedders P A & Drabold D A, *Phys Rev B*, 56 (1997) 1864.
10 Theil J, Lefforge D, Kooi G, Cao M & Ray G W, *J Non-Cryst Solids*, 266/269 (2000) 569.
11 Tsuo Y S, Wang T H & Ciszek T F, *Crystalline-Silicon Solar Cells for the 21st Century, NREL*, Washington, May 3, 1999.
12 Findikoglu A T, Choi W, Matias V, Holesinger T G, Jia Q X & Peterson D E, *Adv Mater*, 17 (2005) 1527.
13 Kim C G, *J Vac Sci Technol B*, 18 (2000) 2650.
14 Teplin C W, Ginley D S & Branz H M, *J Non-Cryst Solids*, 352 (2006) 984.
15 Street R A, Hydrogenated amorphous silicon, © *Cambridge University Press*, 1991.
16 Kosteski T, Kherani N P, Gaspari F, Zukotynski S & Shmayda W T, *J Vac Sci Technol A*, 16 (1998) 893.
17 Stangl R, Froitzheim A & Fuhs W, *European PV Conference, Rome*, Oct.2002.
18 Karim K S, Nathan A & Rowlands J A, *IEEE Trans Electron Dev*, 50 (2003) 200.
19 Long K, Kattamis A Z, Cheng I C, Gleskova H, Wagner S & Sturm J C, *IEEE Electron Dev Lett*, 27 (2006) 111.
20 Kim S, Lee C Y & Jin M H C, *Sol Energy Mater Sol Cells*, 100 (2012) 61.
21 Mensing G, Gilligan J, Hari P, Hurt E, Lupke G, Pantelides S, Tolk N & Taylor P C, *J Non-Cryst Solids*, 299/302 (2002) 621.
22 Thevaril J J & O'Leary S K, *Solid State Commun*, 150 (2010) 1851.
23 Conwaya N M J, Ferrari A C, Flewitt A J, Robertson J, Milne W I, Tagliaferro A & Beyer W, *Diamond Rel Mater*, 9 (2000) 765.
24 Nadazdy V, Durny R & Zeman M, *J Non-Cryst Solids*, 352 (2006) 1059.

25 Kamei T, Stradins P & Matsuda A, *Appl Phys Lett*, 74 (1999) 1707.
26 Rao S V S N, Dixit S K, Lupke G, Tolk N H, Feldman L C, *Phys Rev B*, 75 (2007) 2352021.
27 Peercy P S, *Nucl Instrum Methods*, 182/183 (1981) 337.
28 Jackson W B & Tsai C C, *Phys Rev B*, 45 (1992) 6564.
29 Kroll U, Meier J, Shah A, Mikhailov S & Weber J, *J Appl Phys*, 80 (1996) 4971.
30 Mackenzie K D, Eggert J R, Leopold D J, Li Y M, Lin S & Paul W, *Phys Rev B*, 31 (1985) 2198.
31 Conde J P, Gonçalves M, Brogueira P & Schotten V, *Phys Rev B*, 53 (1996) 1886.
32 Phuong N M, Seong N, Ahn J, Kim E, Lee J, Kim G H & S. Yoon, *Electrochem Solid-State Lett*, 10 (2007) H284.
33 Ozturk M C & Thompson M G, *Appl Phys Lett*, 44 (1984) 916.
34 Drusedau T, Eckler M & Bindemann R, *phys stat sol (a)*, 108 (1988) 285.
35 Tabata A, Nakano J, Mazaki K & Fukaya K, *J Non-Cryst Solids*, 356 (2010) 1131.
36 Guo L, Ding J, Yang J, Ling Z, Cheng G, Yuan N & Wang S, *Vacuum*, 85 (2011) 649.
37 Saha J K, Bahardoust B, Leong K, Gougam A B, Kherani N P & Zukotynski S, *Thin Solid Films*, 519 (2011) 2863.
38 Liu S, Zeng X, Peng W, Xiao H, Yao W, Xie X, Wang C & Wang Z, *J Non-Cryst Solids*, 357 (2011) 121.
39 Dussan A, Quiroz H P & Martinez J G, *Sol Energy Mater Sol Cells*, 100 (2012) 53.
40 Kim J, Abou-Kandil A I, Hong A J, Saad M M, Sadana D K & Chen T, *Appl Phys Lett*, 99 (2011) 062102.
41 Rath J K, Fuhs W & Mell H, *phys stat sol (b)*, 179 (1993) 83.
42 Liao N M, Li W, Jiang Y D, Wu Z M, Li S B, Liu Z, Li Z, Jin X & Chen Y X, *J Phys D: Appl Phys*, 41 (2008) 5412.
43 Koga K, Nakahara K, Kim Y, Kawashima Y, Matsunaga T, Sato M, Yamashita D, Matsuzaki H, Uchida G, Kamataki K, Itagaki N & Shiratani M, *phys stat sol (c)*, 8 (2011) 3013.
44 Yang J, Banerjee A & Guha S, Appl. Phys. Lett. 70 (1997) 2975.
45 Deng X, Liao X, Han S, Povolny H & Agarwal P, *Sol Energy Mater Sol Cells*, 62 (2000) 89.
46 Gordijn A, Zambrano R J, Rath J K & Schropp R E I, *IEEE Trans Electron Dev*, 49 (2002) 949.
47 Estes M J, Hirsch L R, Wichart S & Moddel G, *J Appl Phys*, 82 (1997) 1832.
48 Desalvo A, Giorgis F, Pirria C F, Tresso E, Rava P, Galloni R, Rizzoli R & Summonte C, *J Appl Phys*, 81 (1997) 7973.
49 Patil S B, Kumbhar A A, Saraswat S & Dusane R O, *Thin Solid Films*, 430 (2003) 257.
50 Nawaz M, *J Phys D: Appl Phys*, 44 (2011) 5105.
51 Chen Y, Fang H & Yeh C, *J Non-Cryst Solids*, 357 (2011) 1.
52 Nicolas S M, Munoz D, Ozanne A S, Nguyen N & Ribeyron P J, *Energy Procedia*, 8 (2011) 226.
53 Radue C, Dyk E E V, *Sol Energy Mater Sol Cells*, 94 (2010) 617.
54 Anutgan T A, Anutgan M, Atilgan I, Katircioglu B, *J Non-Cryst Solids*, 356 (2010) 1102.
55 Lipovsek B, Joskowiak A, Krc J, Topic M, Prazeresd D M F, Chu V & Conde J, *Sens Actuat A*, 163 (2010) 96.
56 Swain B P, Swain B S, Chung Y & Hwang N M, *Solid State Sci*, 11 (2009) 1408.
57 Roy B, Mahan A H, Wang Q, Reedy R, Readey D W & Ginley D S, *Thin Solid Films*, 516 (2008) 6517.
58 Munyeme G, Chinyama G K, Zeman M, Schropp R I & Weg W F, *phys stat sol (c)*, 5 (2008) 606.
59 Stiebig H, Moulin E & Rech B, *Thin Solid Films*, 515 (2007) 7522.
60 Meier J, Dubail S, Fluckiger R, Fischer D, Keppner H & Shah A, *Proc.1st WCPEC, Hawaii, U.S.A.*, Dec. 5-9 (1994) 409.
61 Jagannathan B & Anderson W A, *Sol Energy Mater Sol Cells*, 44 (1996) 165.
62 Park S, Baik S, Im J, Fang L, Jeon J & Lim K, *Appl Phys Lett*, 99 (2011) 063504.
63 Hu Y H, Xu H J, Gao H, Chen Y C, Wang L F & Jiang W H, *J Phys: Conf Ser*, 276 (2011) 012167.
64 Ni J, Zhang J, Cao Y, Wang X, Li C, Chen X, Geng X & Zhao Y, *Chin Phys B*, 20 (2011) 087309.
65 Caputo D & Cesare G, *Sens Actuat*, 78 (1999)108.
66 Nathan A, Park B, Ma Q, Sazonova A & Rowlands J A, *Microelectron Reliab*, 42 (2002) 735.
67 Han D & Wang K, *Sol Energy Mater Sol Cells*, 78 (2003) 181.
68 Luterova K, Knapek P, Stuchlik J, Kocka J, Poruba A, Kudrna J, Maly P, Valenta J, Dian J, Honerlage B & Pelant I, *J Non-Cryst Solids*, 227/230 (1998) 254.
69 Liu M, He Y & Jiang X, *NanoStruct Mater*, 10 (1998) 257.
70 Timoshenko V Y, Gonchar K A, Mirgorodskiy I V, Maslova N E, Nikulin V E, Mussabek G K, Taurbaev Y T, Svanbayev E A & Taurbaev TI, *Nanoscale Res Lett*, 6 (2011) 349.
71 Meiling H, Brockhoff A M, Rath J K & Schropp R E I, *J Non-Cryst Solids*, 227/230 (1998) 1202.
72 Martin T, Christou A & Peckerar M, *CS Mantech Conf, Palm Springs,* California, USA, May 16-19, 2011.
73 Indluru A, Venugopal S M, Allee D R & Alford T L, *J Display Technol*, 7 (2011) 306.
74 Caputo D, Cesare G D, Nascetti A & Tucci M, *Sensors Actuat A*, 153 (2009) 1.
75 Lipovsek B, Joskowiak A, Krc J, Topic M, Prazeres D M F, Chu V & Conde J P, *Sensors Actuat A*, 163 (2010) 96.
76 Akaoglu B, Sel K, Atilgan I & Katircioglu B, *Opt Mater*, 30 (2008) 1257.
77 Gosalvez M A, Zubel I & Viinikka E, *Handbook of Silicon Based MEMS Materials and Technologies, 1st ed.,* 2010, pp. 375-407.
78 Williams D E, *Conduction and gas response of semiconductor gas sensors, in: Solid State Gas Sensors, Springer*, Adam Hilger, 1987, p. 71.
79 Helwig A, Muller G, Sberveglieri G & Fagila G, *IEEE Sens J*, 3 (2007) 1506.
80 Wyrsch N, Miazza C, Dunand S, Ballif C, Shah A, Despeisse M, Moraes D, Powolny F & Jarron P, *J Non-Cryst Solids*, 352 (2006) 1797.
81 Negru R & Bonnassieux Y, *J Non-Cryst Solids*, 354 (2008) 2619.
82 Chopra K L, Paulson P D & Dutta V, *Prog Photovolt: Res Appl*, 12 (2004) 69.
83 Keye B, *National solar technology roadmap: film silicon PV, NREL/MP-520-41734*, June 2007.
84 Street R A, *Solar Cells*, 24 (1988) 211.
85 Muller G, Krotz G, Kalbitzer S & Greaves G N, *Philos Mag B*, 69 (1994) 177.
86 Longeau C & Optoelectron J, *Adv Mater*, 4 (2002) 461.
87 Funde A M, Bakr N A, Kamble D K, Hawaldar R R, Amalnerkar D P & Jadkar S R, *Sol Energy Mater Sol Cells*, 92 (2008) 1217.

88 Kocka J, Stuchlikova H, Ledinsky M, Stuchlik J, Mates T & Fejfar A, *Sol Energy Mater Sol Cells*, 93(2009)1444.
89 Zuo ZW, Guan W T, Wang Y, Lu J, Wang J Z, Pu L, Shi Y, Zheng Y D, Luo X Y & Wang H H, *Appl Phys Lett*, 98 (2011) 041902.
90 Knipp D, Chan K, Gordijn A, Marinkovic M & Stiebig H, *J Appl Phys*, 109 (2011) 024504.
91 Staebler D L & Wronski C R, *Appl Phys Lett*, 31 (1977) 292.
92 Pensl G, Roos G, Stoltz P, Johnson N M & Holm C, *Mat Res Soc Symp Proc*, 104 (1988) 241.
93 Zhang S B & Chadi D J, *Phys Rev B*, 41 (1990) 3882.
94 Wang S L & Tayler P C, *AIP Conf Proc (PV Program Review)*, 1995.
95 Wang S L, Viner J M, Anani M & Tayler P C, *J Non-Cryst Solids*, 164/166 (1993) 251.
96 Rath J K, Hackenbuchner B, Fuhs W & Mell H, *Amorphous Silicon Materials and Solar Cells, American Inst. of Physics Conf Proc*, 1991, pp. 98.
97 Kakalios J, *J Non-Cryst Solids*, 114 (1989) 714.
98 Hamed A & Fritzsche H, *J Non-Cryst Solids*, 114 (1989) 717.
99 Hamed A, *Phys Rev B*, 44 (1991) 5585.
100 Hamed A & Fritzsche H, *Philos Mag B*, 65 (1992) 79.
101 Peale R E, Muro K & Sievers AJ, *Mater Sci Forum*, 65/66 (1990) 151.
102 Pensl G, Roos G, Holm C, Sirtl E & Johnson N M, *Appl Phys Lett*, 51 (1987) 451.
103 Wang S L & Taylor P C, *Solid State Commun*, 95 (1995) 361.
104 Yoon J H, Taylor P C & Lee C H, *J Non-Cryst Solids*, 227/230 (1998) 324.
105 Sharma S K, Kumar K N P, Kang K J & Mehra R M, *J Non-Cryst Solids*, 355 (2009) 1638.
106 Sharma S K, Sagar P, Gupta H, Kumar R & Mehra R M, *Solid State Electron*, 51 (2007) 1124.
107 Sharma S K, Baveja J & Mehra R M, *phys stat sol (a)*, 194 (2002) 216.
108 Sharma S K, Baveja J & Mehra R M, *Int J Electron*, 90 (2003) 423.
109 Sharma S K, Gupta H, Purohit L P, Kumar K N P, Kim B, Kumar R & Mehra R M, *J Alloys Compd*, 509 (2011) 3338.
110 Meiling H, Brockhoff A M, Rath J K &, Schropp R E I, *J Non-Cryst Solids*, 227/230 (1998) 1202.
111 Mori M, Tabata, A & Mizutani T, *Thin Solis Films*, 501 (2006) 177.
112 Dusane R O, Dusane S R & Bhide V G, *J Non-Cryst Solids*, 137/138 (1991) 115.
113 Mehra R M, Baveja J, Mathur P C & Taylor PC, *Thin Solid Films*, 312 (1998) 170.
114 Xiong F, Wang Y Y, Leppert V & Chang R P H, J Mater Res, 8 (1993) 2265.
115 Kazushi S, Ryota O, Tomohiro Y, You N, Satoshi M & Tsuyoshi Y, *Diamond Relat Mater*, 19 (2010) 618.
116 Kumarakuru H, Cherns D & Fuge G M, Surf Coat Tech, 205 (2011) 5083.
117 Wang L, Zhang G, Wang Y, Wang Y, Sun X & Xue Q, *J Non-Cryst Solids*, 358 (2012) 65.
118 Fasaki I, Kandyla M, Tsoutsouva M G & Kompitsas M, *Sensor Actuat B: Chem*, 176 (2013) 103.
119 Lengsfeld P, Nickel N H & Fuhs W, *Appl Phys Lett*, 76 (2000) 1680.
120 Mehra R M, Baveja J, Purohit L P, Kumar R, Singh A V, Mathur P C & Taylor P C, *J Non-Cryst Solids*, 266/269, 708 (2000).
121 Al-Dallal S, Aljishi S, Hammam M, Alawi S M A, Stutzmann M, Jin S, Muschik T & Schwarz R, *J Appl Phys*, 70 (1991) 4926.
122 Germer L H & White A W, *Phys Rev*, 60 (1941) 447.
123 Piggott M R, *J Appl Phys*, 37 (1966) 2927.
124 Bernal J D, *Nature*, 183 (1959) 141 & 185 (1960) 68.
125 Zacharison W H, *J Am Chem Soc*, 54 (1932) 3841.
126 Valenkov N & Koshits E P, *Z Krist*, 95 (1937) 195.
127 Mott N F & Gurney R W, *Rept Progr Phys*, 5 (1938) 46.
128 Laaziri K, Kycia S, Roorda S, Chicoine M, Robertson J L, Wang J & Moss S C, *Phys Rev B*, 60 (1991) 13520.
129 Tarkan H M, Gelinas S & Finch J A, *J Colloid Interf Sci*, 297 (2006) 732.
130 Iqbal Z & Veprek S, *J Phys C: Solid State Phys*, 15 (1982) 377.
131 Chase D B, *J Am Chem Soc*, 108 (1986) 7485.
132 Murali M K, & Balachandran, *Indian J Pure & Appl Phys*, 50 (2012) 19.
133 Arivazhagan M & Kavitha R, *Indian J Pure & Appl Phys*, 50 (2012) 709.
134 Zhong Z T, Wang D W, Liao X B, Mou S M, Li C F & Fan Y, *J Non-Cryst Solids*, 134 (1991) 141.
135 Sheng S, Sacher E & Yelon A, *J Non-cryst Solids*, 282 (2001) 165.
136 Toneva A, Marinova T & Krastev V, *J Lumin*, 80 (1998) 455.
137 Yelon A, Rochefort A, Sheng S & Sacher E, *Sol. Energy Mater Sol Cells*, 78 (2003) 391.
138 Lelievre J F, Fourmond E, Kaminski A, Palais O, Ballutaud D & Lemiti M, *Sol Energy Mater Sol Cells*, 93 (2009) 1281.
139 Molinari M, Rinnert H & Vergnat M, *Physica E: Low-dim Sys Nanostruct*, 16 (2003) 445
140 Anandan C, *Appl Surf Sci*, 89 (1995) 57.
141 Sheng S, Hao H, Diao H, Zeng X, Xu Y, Liao X, Monchesky T L, *Appl Surf Sci*, 253 (2006) 1677.
142 Sharma S K, Ph. D thesis entitled "*Investigation of transport mechanism and thermal equilibration in a-Si:H films doped with chalcogens*", *awarded by University of Delhi*, India, 2005.
143 Sharma S K, Kim D Y & Mehra R M, *J. Korean Phys. Soc.*, 62 (2013) 1269.
144 Mehra R M, Inderbir, Jasmina & Mathur P C, *J Non-Cryst Solids*, 209 (1997) 188.
145 Poelman D & Smet P F, *J Phys D: Appl Phys*, 36 (2003) 1850.
146 Nasr A M & Sadik A M, *J Opt A: Pure Appl Opt*, 3 (2001) 200.
147 Caliendo C, Verona E & Saggio G, *Thin Solid Films*, 292 (1977) 255.
148 Swanepoel R, *J Phys E: Sci Instrum*, 16 (1983) 1214.
149 Swanepoel R, *J Phys E: Sci Instrum*, 17 (1984) 896.
150 Anderson B S, Anderson R L, *Fundamentals of Semiconductor Devices, McGraw-Hill Comp Inc*, New York-10020, ©, 2005.
151 Chambouleyron I, Martinez J M, Moretti A C & Mulato M, *Appl Opt*, 36 (1997) 8238.
152 Jellison G E & Modine F A, *Appl Phys Lett*, 69 (1996) 371.
153 Mullerova J, Prusakova L, Netrvalova M, Vavrunkova V & Sutta P, *Appl Surf Sci*, 256 (2010) 5667.

154 Wei W, Jin C, Narayana J & Narayan R J, *Solid State Commn*, 149 (2009) 1670.
155 Bhatt R, Ganesamoorthy S, Bhaumik I, Karnal A K & Gupta P K, *J Phys Chem Solids*, 73 (2012) 257.
156 Gupta R K, Serbetc Z & Yakuphanogluc F, *J Alloys Compd*, 515 (2012) 96.
157 Rawat A, Mahavar H K, Chauhan S, Tanwar A & Singh P J, *Indian J Pure & Appl Phys*, 50 (2012) 100.
158 Das M & Sarkar D, *Indian J Pure & Appl Phys*, 51 (2013) 724.
159 Hussain K M A, Podder J, Saha D K & Ichimura M, *Indian J Pure & Appl Phys*, 50 (2012) 117.
160 Frederiksen J T, Melcher P G & Veje E, *Phys Rev B*, 58 (1998) 8020.
161 Al-Dallal S, Hammam M & Al-Alawi S M, *Phil Mag B*, 64 (1991) 839.
162 Shur M, *Physics of semiconductor devices, Prentice Hall, Englewood Cliffs*, New Jersey, 1990.
163 Pikhtin AN & Yaskov A D, *Sov Phys Semicond*, 14 (1980) 389.
164 Smith Z E, Chu V, Shepard K, Aljishi S, Slobodin D, kolodzy J, Wagner S & Chu T L, *Appl Phys Lett*, 50 (1987) 1521.
165 Ganguly G, Nishio H & Matsuda A, *Appl Phys Lett*, 64 (1994) 3581.
166 Street R A, *Hydrogenated amorphous silicon, Cambridge Solid State Science Series, Cambridge University Press*, (1990), pp 169.
167 Meyer W & Neldel H, *Z Tech Phys*, 12 (1937) 588.
168 Mehta N, *Current Opinion Solid State Mate Sci*, 14 (2010) 95.
169 Kotkata M F, *J Non-Cryst Solids*, 358 (2012) 420.
170 Wang J C & Chen Y F, *Appl Phys Lett*, 73 (1998) 948.
171 Stallinga P & Gomes H L, *Organic Electronics*, 6 (2005) 137.
172 Mansouri S, Zorai S & Bourguiga R, *Synthetic Met*, 162 (2012) 231.
173 Fishchuk I I, Kadashchuk A, Ullah M, Sitter H, Sariciftci N S & Bassler H, *J Phys: Conf Ser*, 376 (2012) 012011.
174 Kirbs V, Druesedau T & Fiedler H, *J Phys: Condens Mater*, 2 (1990) 7473.
175 Widenhorn R, Restand A & Bodegom E, *J Appl Phys*, 91 (2002) 6524.
176 Tassis D H, Dimitriadis C A & Valassiades O, *J Appl Phys*, 84 (1998) 2960.
177 Morii K, Matsui T, Tsuda H & Mabuchi H, *Appl Phys Lett*, 77 (2000) 2361.
178 Kumar A, Lal M, Sharma K, Tripathi S K & Goyal N, *Indian J Pure & Appl Phys*, 51 (2013) 251.
179 Guillen C & Herrero J, *J Appl Phys*, 71 (1992) 5479.
180 Tassis D H, Dimitriadis C A, Brini J, Kamarinos G & Birbas A, *J Appl Phys*, 85 (1999) 4091.
181 Papageorgiou D G & Evangelakis G A, *Surf Sci Lett*, 461 (2000) 543.
182 Yoon BG & Lee C, *J Appl Phys*, 60 (1986) 673.
183 Mott N F & Davis E A, *Electron process in non-crystalline materials* (*Clarendon, Oxford*) 1979.
184 Coleridge P T, *J Phys F: Metal Phys*, 2 (1972) 1016.
185 Lee M J G, *Phys Rev*, 187 (1969) 901.
186 Rose A, "*Concept in Photoconductivity and Allied Problems", Wiley Interscience*, New York, 1963.
187 Zou X, Chan Y C, Webb D P, Lam Y W, Hu Y W, Beling C D, Fung S & Weng H M, *Phys Rev Lett*, 84 (2000) 769.
188 Rene E A & J Baixeras, *Phys Rev B*, 30 (1984) 2016.
189 Vaillant F & Jousse D, *Phys Rev B*, 34 (1986) 4088.
190 Merazga A, Tobbeche S, Main C, Al-Shahrani A & Reynolds S, *J Phys: Condens Matter*, 18 (2006) 3721.
191 Schuler N, Hahn T, Schmerler S, Hahn S, Dornich K & Niklas J R, *J Appl Phys*, 107 (2010) 064901.
192 Yoon J, Jang J & Lee C, *J Appl Phys*, 64 (1988) 6591.
193 Zhou J H & Elliott S R, *Phys Rev B*, 48 (1993) 1505.
194 Neetu & Zulfequar, *Indian J Pure & Appl Phys*, 52 (2013) 53.
195 Werner A, Kunst M & Konenkamp R, *Phys Rev B*, 33 (1986) 33.
196 Cloude C, Spear W E, LeComber P G & Hourd AC, *Philos Mag B*, 54 (1986) L113.
197 Spear W E, *Silicon and Related Materials, ed. H. Fritzche, World Scientific*, Singapore, 1989, pp. 721.
198 Spear W E, Loveland R J & Sharbaty A A, *J Non-Cryst Solids*, 15 (1974) 410.
199 Scholl F W, *Rev Sci Instrum*, 51(1980) 1418.
200 Moses D & Heeger A J, *J Phys: Condens Matter*, 1 (1989) 7395.
201 Ogawa N, Nagase T & Naito H, *J Non-Cryst Solids*, 266/269 (2000) 367.
202 Yasuno S, Kita T, Morita S, Kugimiya T, Hayashi K & Sumie S, *J Appl Phys*, 112 (2012) 053715.
203 Ostroverkhova O, Cooke D G, Hegmann F A, Tykwinski R R, Parkin S R & Anthony J E, *Appl Phys Lett*, 89 (2006) 192113.
204 Nalla V, Polavarapu L, Manga K K, Goh B M, Loh K P, Xu Q & Ji W, *Nanotechnology*, 21 (2010) 415203.
205 Cowan S R, Street R A, Cho S & Heeger A J, *Phys Rev B*, 83 (2011) 035205.
206 Yoo B, Song Y, Lee C & Jang J, *Phys Rev B*, 41 (1990) 10787.
207 Theodorou D E & Symeonidis C I, *Phys Rev B*, 37 (1988) 10854.
208 Lee C & Yoo B, *Chin J Phys*, 28 (1990) 37.
209 Amekura H, Kishimoto N, Kono K & Kondo A, *J Non-Cryst Solids*, 266/69 (2000) 444.
210 Sato S, Sai H, Ohshima T, Imaizumi M, Shimazaki K & Kondo M, *J Non-Cryst Solids*, 356 (2010) 2114.
211 Feng P, Monch I, Harazim S, Huang G, Mei Y & Schmidt O G, *Nano Lett*, 9 (2009) 3453.
212 Nayak J, Kasuya J, Watanabe A & Nozaki S, *J Phys: Condens Matter*, 20 (2008) 195222.
213 Hullavarad S, Hullavarad N, Look D & Claflin B, *Nanoscale Res Lett*, 4 (2009) 1421.
214 Bao J, Shalish I, Su Z, Gurwitz R, Capasso F, Wang X & Ren Z, *Nanoscale Res Lett*, 6 (2011) 404.
215 Vavilov V S, Euthymiou P C, Zardas G E, *Phys Uspekhi*, 42 (1999) 199.
216 Zardas G E, Yannakopoulos P H, Ziska M, Symeonides C, Euthymiou P C & Csabay O, *Microelectron J*, 36 (2005) 1.
217 Hung H, Chen C, Chang S J, Kuan H, Lin R M & Liu C H, *J Cryst Growth*, 298 (2007) 246.
218 Tebano A, Fabbri E, Pergolesi D, Balestrino G & Traversa E, *ACS Nano*, 6 (2012) 1278.
219 Pal R K, Agnihotri A K & Kumar A, *Chalcogenide Lett*, 7 (2010) 439.
220 Chaudhary N, Bahishti A A & Zulfequar M, *Physica B*, 407 (2012) 2267.
221 Hsu S H, Su Y K, Chuang R W, Chang S J, Chen W C & Chen W R, *Japan J Appl Phys*, 44 (2005) 2454.

222 Juang F, Shen H & Wang W, *J Electron Mater*, 41 (2012) 2204.
223 Shen J L, Lee Y C, Shu G W, Chou W C & Uen W Y, *Semicond Sci Technol*, 17 (2002) L72.
224 Meyer T, Engelhardt F, Parisi J & Raua U, *J Appl Phys*, 91 (2002) 5093.
225 Ursaki V V, Tiginyanu I M, Riccia P C, Anedda A, Hubbard S & Pavlidis D, *J Appl Phys*, 94 (2003) 3876.
226 Lang D V & Logan R A, *Phys Rev Lett*, 39 (1977) 635.
227 Mooney P M, Caswell N S & Wright S L, *J Appl Phys*, 62 (1987) 4786.
228 Queisser H J & Theodoru D E, *Phys Rev B*, 33 (1986) 4027.
229 Jiang H X & Lin J Y, *Phys Rev B*, 40 (1989) 10025.
230 Kakalios J & Fritzsche H, *Phys Rev Lett*, 53 (1984) 1602.
231 Choi S, Park G, Lee C & Jang J, *Solid State Commun*, 59 (1986) 177.
232 Wang S L & Taylor P C, *AIP Conf Proc*, 353 (1996) 487.
233 Taylor P C, *Characterization of amorphous silicon thin films and PV devices*, NREL/ SR-520-31984, March 2002.
234 Crandall R & Luft W, *Prog Photovol Res Appl*, 3 (1995) 315.
235 Jennings P J, Cornish J C L, Clare B W, Hefter G T & Santjojo D J, *Thin Solid Films*, 310 (1997) 156.
236 Rujanapich P, Poyai A, Srithanachai I, Ueamanapong S & Titiroongruang W, *Indian J Pure & Appl Phys*, 51 (2013) 587.